A linear second-order in time unconditionally energy stable finite element scheme for a Cahn-Hilliard phase-field model for two-phase incompressible flow of variable densities

Guosheng Fu<sup>1</sup>, Daozhi Han<sup>2</sup>.

#### Abstract

We propose a novel second—order BDF time stepping method of variable time step sizes combined with a classical residual-based stabilized finite element spatial discretization using the Streameline-Upwind Petrov-Galerkin (SUPG)/pressure stabilization Petrov-Galerkin (PSPG)/grad-div stabilization for solving the phase—field model for two—phase incompressible flow of different densities and viscosities in the advection dominated regime. In the case of uniform time step size and without extra stabilization, the scheme is shown to satisfy a discrete energy law. Benchmark test of the Rayleigh—Taylor instability under high Reynolds number and Péclect number demonstrates that the scheme captures details of the instability comparable to results in the literature by schemes based on sharp-interface models.

**Keywords**— Cahn-Hilliard-Navier-Stokes; two-phase incompressible flow; energy law preserving; stabilized finite element method

## 1. Introduction

Phase field fluid models play increasingly important roles in the study of multiphase flows, owing to their flexibility in modeling multi-physics, the ease of capturing moving boundaries in numerical simulations, and the built-in physical mechanism (chemical diffusion) allowing smooth topological changes of interfaces, cf. [3, 47] for some applications of phase field fluid models. In this work, we focus on solving numerically the two-phase incompressible flow problem of variable densities and viscosities using the thermodynamically consistent Cahn-Hilliard phase-field model proposed by Abels et al. [1], see also [42]. Compared to the quasi-incompressible two-phase flow model developed by Lowengrub and Truskinovsky [55], volume-averaged velocity is adopted in this model hence the velocity field of the mixture remains solenoidal.

<sup>&</sup>lt;sup>1</sup>Department of Applied and Computational Mathematics and Statistics, University of Notre Dame, Notre Dame, IN 46556, USA. Email: gfu@nd.edu.

<sup>&</sup>lt;sup>2</sup>Department of Mathematics & Statistics, Missouri University of Science and Technology, Rolla, MO 65409, USA. Email: handaoz@mst.edu

A major challenge in solving phase field fluid models is the stiffness associated with the diffusive interface (sharp transition of field variables in thin layers). Energy-law preserving hence unconditionally stable time marching schemes are desired for solving these systems so that stiffness can be resolved adaptively without suffering from a severe CFL constraint. Many approaches have been proposed in recent years, including the convex-concave splitting method [20, 21, 59, 25], the stabilized linear approach [62], the Invariant Energy Quadratization (IEQ) method [30, 68, 67, 26], and the Scalar Auxiliary Variable (SAV) approach [60, 61]. Applications of these methods to phase field fluid models can be found in [46, 36, 23, 34, 63, 33, 19, 72, 32, 27] among many others.

There are several numerical methods for solving the phase field model for incompressible two-phase flow of variable densities. In [31] a first-order energy-law preserving scheme is developed in which the Cahn-Hilliard solver is decoupled from the Navier-Stokes solver via a fractional step method, see also [63]. A second-order accurate, coupled, energy-law preserving linear scheme is proposed in [27] based on the Crank-Nicolson method and the IEQ approach. In this second-order accurate method, periodic boundary condition is necessary for establishing energy stability of the fully discrete scheme since the scheme utilizes a scaled velocity variable in the Crank-Nicolson discretization. Separately, a totally decoupled, second-order accurate, unconditionally stable numerical method is constructed in [69]. The key idea in this method is the introduction of two SAVs: one for linearizing the Cahn-Hilliard solver, the other one for canceling out the explicitly discretized nonlinear terms in the energy estimate. The method is computationally efficient since the only nonlinear equation involved is a low order polynomial for a scalar variable, and the coefficient matrices are precomputable. We point out that linear versions of the method in [69] can be readily derived by using variants of the SAV approach recently developed in [70, 66, 49]. It should be noted that despite the unconditional stability of these SAVbased schemes the time step size needs to be relatively small for meaningful numerical simulations in the case of large Péclet number and constant mobility. One possible explanation for it is that the CFL condition might be still necessary in the advection-dominated regime due to explicit treatment of the advection terms in these schemes.

In this article we aim to solve the incompressible two-phase flow model of variable densities in the advection-dominated regime (large Péclet number and Reynolds number) with a degenerate mobility function. The degenerate mobility function implies that the order parameter remains in its physical bounds, which is essential for two-phase flows of arbitrary densities and viscosities. Moreover, thanks to the degenerate mobility, the un-physical effect of bulk diffusion for two-phase flows is reduced/delayed to a large time scale [16, 48]. Solving the Cahn-Hilliard equation with a degenerate mobility function is very challenging [8]. Indeed, our numerical tests have shown that with a degenerate mobility function the SAV variable of the decoupled scheme in [66] deviates significantly from its true value, regardless of smallness of the time step size, which in turn contributes to an order one consistency error to the modified PDEs. A second challenge is that in

the advection-dominated regime the diffusive interface behaves much like a viscous shock. It is known that traditional high-order methods can produce spurious oscillations near diffusive interfaces (analogous to the Gibbs phenomenon) which can pollute the numerical solution beyond the sharp transition layers, cf. [24]. To address these challenges we propose a second-order BDF time-stepping method of variable time step size effected with SUPG/PSPG/grad-div stabilized continuous finite elements for the spatial discretization. The scheme with uniform time step size and without extra stabilization is shown to satisfy a discrete energy law. Extensive benchmark simulations of the Rayleigh-Taylor instability under high Reynolds number and Péclet number show that the scheme captures details of the instability comparable to those by sharp interface model-based numerical methods. In particuler, the numerical results demonstrate that the stabilized scheme is more robust than the plain Galerkin method without extra stabilization in the high Reynolds number and Péclect number regime.

We will not pursue convergence analysis/error estimates of the proposed numerical schemes, but verify convergence through numerical experiments in this article. Convergence analysis for the Cahn-Hilliard-Navier-Stokes (Darcy) equations can be found in [18, 19, 10, 54, 9]. In addition, there have been many developments on BDF2/BDF3 methods for various gradient flow models, cf. [65, 12, 22, 13, 56, 35].

The rest of the article is organized as follows: in Sec. 2 we introduce the model, present the time-stepping method and the spatial discretization; numerical results are reported in Sec. 3; we conclude in Sec. 4 with a brief summary and some further discussions.

## 2. The model and discretization

## 2.1. The model

We consider the following thermodynamically consistent Cahn-Hilliard phase-field model of Abels et al. [1] for incompressible two-phase flow in the domain  $\Omega \subset \mathbb{R}^d$ , d=2,3:

$$\partial_{t}(\rho(\phi)\mathbf{u}) + \nabla \cdot (\mathbf{u} \otimes (\rho(\phi)\mathbf{u} + \mathbf{J})) + \nabla p - \nabla \cdot (2\eta(\phi)\mathbb{D}(\mathbf{u})) + \tilde{\sigma}\epsilon\nabla \cdot (\nabla\phi \otimes \nabla\phi) = \mathbf{f},$$
(1a)
$$\nabla \cdot \mathbf{u} = 0,$$
(1b)
$$\partial_{t}\phi + \nabla \cdot (\phi\mathbf{u}) - \nabla \cdot (M(\phi)\nabla\mu) = 0,$$
(1c)
$$\mu - \frac{\tilde{\sigma}}{\epsilon}(F'(\phi) - \epsilon^{2}\Delta\phi) = 0,$$
(1d)
$$\mathbf{J} - \frac{\rho_{1} - \rho_{2}}{2}M(\phi)\nabla\mu = 0.$$
(1e)

Here

$$\rho(\phi) := \frac{\rho_1 + \rho_2}{2} + \frac{\rho_2 - \rho_1}{2}\phi$$

is the density with  $\phi$  being an order parameter related to the concentration of the fluids and  $\rho_j > 0$  being the specific (constant) density of fluid j = 1, 2,  $\mathbf{u}$  is the mean velocity, p is the pressure,  $\mathbb{D}(\mathbf{u}) = \frac{1}{2}(\nabla \mathbf{u} + \nabla \mathbf{u}^T)$ ,  $\mathbf{f}$  is the source term,

$$\eta(\phi) := \frac{\eta_1 + \eta_2}{2} + \frac{\eta_2 - \eta_1}{2}\phi$$

is the viscosity of the mixture with  $\eta_j > 0$  being the specific (constant) viscosity of fluid j = 1, 2,

$$\tilde{\sigma} := \frac{3}{2\sqrt{2}}\sigma$$

is the scaled surface tension with  $\sigma$  being the physical surface tension,  $\epsilon > 0$  is a (small) parameter related to the thickness of the interfacial region,  $M(\phi)$  is the mobility function,  $\mu$  is the chemical potential,  $F(\phi)$  is the free energy density, and  $\mathbf{J}$  is the relative flux related to diffusion of the components. In this work, we consider the following double well potential for the free energy density, and a degenerate mobility:

$$F(\phi) := \frac{(\phi^2 - 1)^2}{4}, \quad M(\phi) := \gamma(\phi^2 - 1)^2,$$
 (1f)

where  $\gamma$  is the mobility coefficient. Another popular choice for the mobility function is  $M(\phi) = \gamma(1-\phi^2)$ . The qualitative behavior of the solution may strongly depend on the degeneracy order of the mobility function, as suggested by recent study in [57, 16, 17]. In this article we will utilize the model both in its dimensional form as in (1) and its dimensionless form with Pe the diffusional Péclet number (measure of advection over chemical diffusion) and Re the classical Reynolds number. We refer to [55, 45] for details of the non-dimensionalization.

We close this system with the following initial and boundary conditions

$$\mathbf{u} = 0, \quad \text{on } \partial\Omega \times (0, T)$$
 (2a)

$$\nabla \phi \cdot \mathbf{n} = \nabla \mu \cdot \mathbf{n} = 0, \quad \text{on } \partial \Omega \times (0, T)$$
 (2b)

$$(\mathbf{u}, \phi)|_{t=0} = (\mathbf{u}_0, \phi_0), \quad \text{in } \Omega.$$
 (2c)

Here **n** denotes the unit outer normal vector of the boundary  $\partial\Omega$ . It can be shown that the system (1) under the above boundary conditions satisfies the following energy law:

$$\frac{d}{dt}E_{tot}(\mathbf{u},\phi) = -\int_{\Omega} 2\nu(\phi)\mathbb{D}(\mathbf{u}) : \mathbb{D}(\mathbf{u}) dx - \int_{\Omega} M(\phi)|\nabla \mu|^2 dx + \int_{\Omega} \mathbf{f} \cdot \mathbf{u} dx, \qquad (3)$$

where the total energy  $E_{tot}$  is defined as

$$E_{tot}(\mathbf{u}, \phi) = \int_{\Omega} \frac{1}{2} \rho(\phi) |\mathbf{u}|^2 d\mathbf{x} + \int_{\Omega} \frac{\widetilde{\sigma}}{\epsilon} \left( F(\phi) + \frac{\epsilon^2}{2} |\nabla \phi|^2 \right) dx.$$

Here we focus on the no-slip no penetration boundary condition (2a) so that the energy identity (3) holds. Other boundary conditions such as outflow or open boundary conditions can be treated using the recently developed generalized Positive Auxiliary Variable approach for maintaining energy stability. We refer to [53] for details.

By introducing the following modified pressure

$$P := p + \frac{\widetilde{\sigma}}{\epsilon} \left( F(\phi) + \frac{1}{2} \epsilon^2 |\nabla \phi|^2 \right) - \phi \mu, \tag{4}$$

the momentum equation (1a) can be reformulated as

$$\partial_t(\rho(\phi)\mathbf{u}) + \nabla \cdot (\mathbf{u} \otimes (\rho(\phi)\mathbf{u} + \mathbf{J})) + \nabla P - \nabla \cdot (2\eta(\phi)\mathbb{D}(\mathbf{u})) + \phi \nabla \mu = \mathbf{f}, \tag{5}$$

By the definition of the density, the relative flux in (1e), and equation (1c), we have

$$\partial_t \rho(\phi) + \nabla \cdot (\rho(\phi)\mathbf{u} + \mathbf{J}) = 0.$$

Follow the idea in [28], we multiply the above identity with  $\frac{1}{2}\mathbf{u}$  and subtract from the momentum equation (5) to get

$$\partial_t(\rho(\phi)\mathbf{u}) + \nabla \cdot (\mathbf{u} \otimes (\rho(\phi)\mathbf{u} + \mathbf{J})) + \nabla P - \nabla \cdot (2\eta(\phi)\mathbb{D}(\mathbf{u})) + \phi \nabla \mu - \frac{1}{2}\mathbf{u} \left(\partial_t \rho(\phi) + \nabla \cdot (\rho(\phi)\mathbf{u} + \mathbf{J})\right) = \mathbf{f},$$

which can be simplified as

$$\sqrt{\rho(\phi)}\partial_t(\sqrt{\rho(\phi)}\mathbf{u}) + \left(\nabla \cdot (\mathbf{u} \otimes (\rho(\phi)\mathbf{u} + \mathbf{J})) - \frac{1}{2}\mathbf{u} \nabla \cdot (\rho(\phi)\mathbf{u} + \mathbf{J})\right) + \nabla P - \nabla \cdot (2\eta(\phi)\mathbb{D}(\mathbf{u})) + \phi \nabla \mu = \mathbf{f}.$$
(6)

It is clear that the equation (6), combined with equations (1b)–(1e) is mathematically equivalent to the original system (1).

Remark 2.1 (On energy stability). The energy identity (3) can be directly obtained by a standard variational approach, where one multiply the equations (6), (1b), (1c), and (1d), with test functions  $\mathbf{u}$ , P,  $\mu$ , and  $\partial_t \phi$ , respectively, add up the resulting terms, and then integrate over the domain  $\Omega$ . Hence, a Galerkin finite element spatial discretization for the equations (6), and (1b)–(1e) is expected to preserve this energy identity in the semi-discrete (continuous in time) case.

To obtain a linear, fully discrete energy stable scheme for the model (1), we follow the recent scalar auxiliary variable (SAV) approach [61, 50] by introducing a scalar variable that only depends on time t:

$$\frac{dU}{dt} = \frac{1}{2} \int_{\Omega} r(\phi) \frac{\partial \phi}{\partial t} dx, \tag{7a}$$

$$U(0) = \sqrt{\int_{\Omega} \left( F(\phi(0)) - \frac{s}{2}\phi(0)^2 \right) dx + B},$$
 (7b)

where

$$r(\phi) = \frac{F'(\phi) - s\phi}{\sqrt{\int_{\Omega} \left(F(\phi) - \frac{s}{2}\phi^2\right) dx + B}},$$
 (7c)

and s > 0 is a user-defined stabilization parameter, B is a positive constant such that U is well-defined. Note that we immediately have

$$U(t) = \sqrt{\int_{\Omega} \left( F(\phi) - \frac{s}{2} \phi^2 \right) dx + B}.$$

With the help of the scalar variable U(t), we rewrite the system (6), (1b)–(1e) as follows:

$$\sqrt{\rho(\phi)}\partial_{t}(\sqrt{\rho(\phi)}\mathbf{u}) + \nabla \cdot (\mathbf{u} \otimes (\rho(\phi)\mathbf{u} + \mathbf{J})) - \frac{1}{2}\mathbf{u} \nabla \cdot (\rho(\phi)\mathbf{u} + \mathbf{J}) + \phi \nabla \mu 
+ \nabla P - \nabla \cdot (2\eta(\phi)\mathbb{D}(\mathbf{u})) = \mathbf{f},$$
(8a)

$$\nabla \cdot \mathbf{u} = 0, \qquad (8b)$$

$$\partial_t \phi + \nabla \cdot (\phi \mathbf{u}) - \nabla \cdot (M(\phi) \nabla \mu) = 0,$$
 (8c)

$$\mu - \frac{\tilde{\sigma}}{\epsilon} (Ur(\phi) + s\phi - \epsilon^2 \Delta \phi) = 0, \quad (8d)$$

$$\mathbf{J} - \frac{\rho_1 - \rho_2}{2} M(\phi) \nabla \mu = 0.$$
 (8e)

It is clear that the system (7)–(8) with boundary conditions (2) is equivalent to the original system (1) with boundary conditions (2). In particular, the following energy stability result holds:

$$\frac{d}{dt}\widetilde{E}_{tot} = -\int_{\Omega} 2\nu(\phi)\mathbb{D}(\mathbf{u}) : \mathbb{D}(\mathbf{u}) \,d\mathbf{x} - \int_{\Omega} M(\phi)|\nabla \mu|^2 \,d\mathbf{x} + \int_{\Omega} \mathbf{f} \cdot \mathbf{u} \,d\mathbf{x}, \tag{9}$$

where the *modified* total energy

$$\widetilde{E}_{tot} := \int_{\Omega} \frac{1}{2} \rho(\phi) |\mathbf{u}|^2 d\mathbf{x} + \int_{\Omega} \frac{\widetilde{\sigma}}{\epsilon} \left( \frac{s}{2} \phi^2 + \frac{\epsilon^2}{2} |\nabla \phi|^2 \right) d\mathbf{x} + \frac{\widetilde{\sigma}}{\epsilon} U^2.$$

Note that this modified energy is related to the original one by the identity  $\widetilde{E}_{tot} = E_{tot}(\mathbf{u}, \phi) + \frac{\tilde{\sigma}}{\epsilon}B$ . Our numerical scheme is a discretization of the modified system (7)–(8), which preserve a discrete version of the modified energy identity (9). In the discrete level, the modified energy may not be directly related to the original energy  $E_{tot}(\mathbf{u}, \phi)$ , which could be a shortcoming of the proposed scheme that is common to all SAV based methods.

## 2.2. The time-marching scheme

Phenomena associated with Cahn-Hilliard phase field fluid models often involve multiple time and spatial scales. Adaptive time-stepping is an important tool for efficient simulation of these phenomena, especially when long-time simulation is of interest, cf. [71, 31, 14, 51, 52] for development in this direction. In this subsection, we discretize the system (7)–(8) in time using the (variable step-size) second-order BDF2 method with Adam-Bashforth extrapolations to arrive at a second-order, unconditionally energy stable (for the modified energy), and linearly coupled time-discretization scheme. A similar BDF scheme of variable steps has been applied to solving the Cahn-Hilliard equation in [11].

Let  $U^0, \mathbf{u}^0, \phi^0, \mu^0$  be the initial data, and let  $0 = t^0 < t^1 < t^2 < \cdots < t^N = T$  be a discretization of the time interval [0, T], with a variable time step size  $\Delta t^j := t^j - t^{j-1}$ . For any  $j \geq 1$ , we denote the difference operator

$$\delta_t \psi^j := \begin{cases} (\psi^1 - \psi^0)/\Delta t^1 & \text{if } j = 1, \\ w_2^j \psi^j + w_1^j \psi^{j-1} + w_0^j \psi^{j-2}, & \text{if } j \ge 2, \end{cases}$$
(10a)

and the extrapolations

$$\widetilde{\psi}^{j} := \begin{cases}
\psi^{0} & \text{if } j = 1, \\
e_{1}^{j} \psi^{j-1} + e_{0}^{j} \psi^{j-2}, & \text{if } j \geq 2,
\end{cases}$$
(10b)

where the (second-order) weights for  $j \geq 2$  are

$$w_2^j = \frac{\Delta t^{j-1} + 2\Delta t^j}{(\Delta t^{j-1} + \Delta t^j)\Delta t^j}, \quad w_1^j = -\frac{\Delta t^{j-1} + \Delta t^j}{\Delta t^{j-1}\Delta t^j}, \quad w_0^j = \frac{\Delta t^j}{\Delta t^{j-1}(\Delta t^{j-1} + \Delta t^j)}, \quad (10c)$$

$$e_1^j = 1 + \frac{\Delta t^j}{\Delta t^{j-1}}, \quad e_0^j = -\frac{\Delta t^j}{\Delta t^{j-1}}.$$
 (10d)

Without loss of generality, we further set  $\widetilde{\psi}^0 := \psi^0$ .

Now our temporal discretization for the system (7)–(8) reads as follows: for any  $j \ge 1$ , find the solution  $U^j, \mathbf{u}^j, \phi^j, \mu^j, P^j$  such that

$$\delta_t U^j - \frac{1}{2} \int_{\Omega} r(\widetilde{\phi}^j) \delta_t \phi^j \, \mathrm{dx} = 0, \tag{11a}$$

$$\sqrt{\rho(\widetilde{\phi}^j)}\delta_t(\sqrt{\rho(\widetilde{\phi}^j)}\mathbf{u}^j) + \nabla P^j - \nabla \cdot \left(2\eta(\widetilde{\phi}^j)\mathbb{D}(\mathbf{u}^j)\right)$$

$$+\nabla \cdot \left(\mathbf{u}^{j} \otimes (\rho(\widetilde{\phi}^{j})\widetilde{\mathbf{u}}^{j} + \widetilde{\mathbf{J}}^{j})\right) - \frac{1}{2}\mathbf{u}^{j} \nabla \cdot (\rho(\widetilde{\phi}^{j})\widetilde{\mathbf{u}}^{j} + \widetilde{\mathbf{J}}^{j}) + \widetilde{\phi}^{j} \nabla \mu^{j} = \mathbf{f}^{j}, \tag{11b}$$

$$\nabla \cdot \mathbf{u}^j = 0, \tag{11c}$$

$$\delta_t \phi^j + \nabla \cdot (\widetilde{\phi}^j \mathbf{u}^j) - \nabla \cdot (M(\widetilde{\phi}^j) \nabla \mu^j) = 0, \tag{11d}$$

$$\mu^{j} - \frac{\tilde{\sigma}}{\epsilon} (U^{j} r(\tilde{\phi}^{j}) + s\phi^{j} - \epsilon^{2} \triangle \phi^{j}) = 0, \tag{11e}$$

where

$$\widetilde{\mathbf{J}}^{j} = \frac{\rho_{1} - \rho_{2}}{2} M(\widetilde{\phi}^{j}) \nabla \widetilde{\mu}^{j}, \tag{11f}$$

and the difference operator term in equation (11b) is

$$\delta_{t}(\sqrt{\rho(\widetilde{\phi}^{j})}\mathbf{u}^{j}) = \begin{cases} (\sqrt{\rho(\widetilde{\phi}^{1})}\mathbf{u}^{1} - w_{1}^{j}\sqrt{\rho(\widetilde{\phi}^{0})}\mathbf{u}^{0})/\Delta t^{1} & \text{if } j = 1, \\ w_{2}^{j}\sqrt{\rho(\widetilde{\phi}^{j})}\mathbf{u}^{j} + w_{1}^{j}\sqrt{\rho(\widetilde{\phi}^{j-1})}\mathbf{u}^{j-1} + w_{0}^{j}\sqrt{\rho(\widetilde{\phi}^{j-2})}\mathbf{u}^{j-2} & \text{if } j \geq 2. \end{cases}$$

$$(11g)$$

It is clear that the above scheme is a fully coupled linear method. Moreover, when the time step size does not change over time, the following unconditional *modified* energy stability result holds.

**Theorem 2.1** (Unconditional energy stability). Assume the time step size  $\Delta t^j = \Delta t$  for all  $j = 1, 2, \dots, N$ , and assume the source term  $\mathbf{f} = 0$ , then the following equality holds for the scheme (11) for  $j \geq 2$ :

$$\widetilde{E}_{tot}^{j} - \widetilde{E}_{tot}^{j-1} = -\Delta t \int_{\Omega} \left( 2\eta(\widetilde{\phi}^{j}) \mathbb{D}(\mathbf{u}^{j}) : \mathbb{D}(\mathbf{u}^{j}) + M(\widetilde{\phi}^{j}) |\nabla \mu^{j}|^{2} \right) d\mathbf{x} - \mathsf{N}^{j}, \tag{12a}$$

where the modified energy at time  $t^{j}$  is given as

$$\widetilde{E}_{tot}^{j} := \frac{1}{4} \left( \int_{\Omega} \rho(\widetilde{\phi}^{j}) |\mathbf{u}^{j}|^{2} dx + \int_{\Omega} \frac{\widetilde{\sigma}}{\epsilon} \left( s(\phi^{j})^{2} + \epsilon^{2} |\nabla \phi^{j}|^{2} \right) dx + \frac{2\widetilde{\sigma}}{\epsilon} (U^{j})^{2} \right) \\
+ \frac{1}{4} \left( \int_{\Omega} \left| 2\sqrt{\rho(\widetilde{\phi}^{j})} \mathbf{u}^{j} - \sqrt{\rho(\widetilde{\phi}^{j-1})} \mathbf{u}^{j-1} \right|^{2} dx + \frac{2\widetilde{\sigma}}{\epsilon} (2U^{j} - U^{j-1})^{2} \right) \\
+ \frac{1}{4} \int_{\Omega} \frac{\widetilde{\sigma}}{\epsilon} \left( s(2\phi^{j} - \phi^{j-1})^{2} + \epsilon^{2} |\nabla(2\phi^{j} - \phi^{j-1})|^{2} \right) dx, \tag{12b}$$

and the non-negative numerical dissipation term is given as

$$\mathbf{N}^{j} := \frac{1}{4} \int_{\Omega} \left| \sqrt{\rho(\widetilde{\phi}^{j})} \mathbf{u}^{j} - 2\sqrt{\rho(\widetilde{\phi}^{j-1})} \mathbf{u}^{j-1} + \sqrt{\rho(\widetilde{\phi}^{j-2})} \mathbf{u}^{j-2} \right|^{2} d\mathbf{x}$$

$$+ \frac{\widetilde{\sigma}}{4\epsilon} (U^{j} - 2U^{j-1} + U^{j-2})^{2}$$

$$+ \frac{1}{4} \int_{\Omega} \frac{\widetilde{\sigma}}{\epsilon} \left( s(\phi^{j} - 2\phi^{j-1} + \phi^{j-2})^{2} + \epsilon^{2} |\nabla(\phi^{j} - 2\phi^{j-1} + \phi^{j-2})|^{2} \right) d\mathbf{x}.$$
(12c)

*Proof.* Multiplying the equations (11a) with test function  $\frac{2\tilde{\sigma}}{\epsilon}U^j$ , and multiplying the equations (11b), (11c), (11d), (11e), (11f) with test functions  $\mathbf{u}^j$ ,  $P^j$ ,  $\mu^j$ ,  $-\delta_t\phi^j$ , respectively, adding the resulting terms, integrating over the domain  $\Omega$  and apply integration-by-parts, we get

$$\frac{2\widetilde{\sigma}}{\epsilon} (\delta_t U^j) U^j + \int_{\Omega} \left( \delta_t (\sqrt{\rho(\widetilde{\phi}^j)} \mathbf{u}^j) \right) \sqrt{\rho(\widetilde{\phi}^j)} \mathbf{u}^j + \frac{\widetilde{\sigma}}{\epsilon} \left( s \phi^j \delta_t \phi^j + \epsilon^2 \nabla \phi^j \cdot \delta_t (\nabla \phi^j) \right) dx$$

$$= -\int_{\Omega} \left( 2\eta(\widetilde{\phi}^{j}) \mathbb{D}(\mathbf{u}^{j}) : \mathbb{D}(\mathbf{u}^{j}) + M(\widetilde{\phi}^{j}) |\nabla \mu^{j}|^{2} \right) d\mathbf{x}, \tag{13}$$

where we specifically mention that the integral of the coupling terms  $\widetilde{\phi}^j \nabla \mu^j \cdot \mathbf{u}^j$  and  $\nabla \cdot (\widetilde{\phi}^j \mathbf{u}^j) \mu^j$  cancels out due to integration by parts and the boundary condition (2a).

Note that for the constant time step case we have  $\delta_t \phi^j = \frac{1}{2\Delta t} (3\psi^j - 4\psi^{j-1} + \psi^{j-2})$  for  $j \geq 2$ . Elementary calculation yields that

$$(\delta_t \psi^j) \psi^j = \frac{1}{4\Delta t} \Big( \left( |\psi^j|^2 + |2\psi^j - \psi^{j-1}|^2 \right) - \left( |\psi^{j-1}|^2 + |2\psi^{j-1} - \psi^{j-2}|^2 \right) + |\psi^j - 2\psi^{j-1} + \psi^{j-2}|^2 \Big).$$

Combining the above identity with the equality (13), we immediately obtain the energy identity (12a). This completes the proof.

Remark 2.2 (On energy stability for variable time stepping). We are not able to give a rigorous proof of energy stability of the scheme (11) for the more general variable time step-size case. For an energy identity it is necessary to multiply the variable time-step BDF2 method (10a) by the difference  $\varphi^j - \varphi^{j-1}$ , which works for the Cahn-Hilliard equation since it is a  $H^{-1}$  gradient flow, cf. [11]. However, one has to test the advective Cahn-Hilliard equation (11d) with  $\mu^j$  in order to cancel out advection term in the Cahn-Hilliard equation with the capillarity term in the fluid equations in the energy estimate.

Remark 2.3 (On decoupled scheme and energy stability). It is generally difficult to construct second-order linear decoupled energy stable schemes for variable density CHNS models due to the nonlinear coupling of phase-field and flow variables. Recently there are some interesting work to construct decoupled energy stable schemes [69, 66] for CHNS models. The work [69] modified the scalar variable to be the square root of the sum of the kinetic energy and the potential free energy, instead of only the potential free energy considered in our work. As a result, the modified energy stability result in [69, Theorem 2.1], which does not contain the "true" kinetic energy, is weaker than ours in Theorem 2.1.

Let us discuss more details on the recent work [66]. We focus on the application of the key idea in [66] to our model (7) and (8). It introduces another auxiliary scalar variable Q(t) to deal with the nonlinear (coupling/convection) terms, which satisfy the following ODE:

$$\frac{dQ}{dt} = \int_{\Omega} \left( \nabla \cdot (\mathbf{u} \otimes (\rho(\phi)\mathbf{u} + \mathbf{J})) - \frac{1}{2}\mathbf{u} \nabla \cdot (\rho(\phi)\mathbf{u} + \mathbf{J}) + \phi \nabla \mu \right) \cdot \mathbf{u} \, d\mathbf{x}$$
$$+ \int_{\Omega} \nabla \cdot (\phi \mathbf{u}) \mu d\mathbf{x},$$

with Q(0) = 1. It is straightforward to verify that the right hand side of the above equation is identically zero as long as  $\mathbf{u} \cdot \mathbf{n} = \mathbf{J} \cdot \mathbf{n} = 0$  on the boundary  $\partial \Omega$ , which is termed as the zero-energy-contribution property in [66]. Hence,  $Q(t) \equiv 1$  for all time. The author in [66] then modified the equations (8a) and (8c) by multiplying the nonlinear terms therein with Q(t) = 1. A linear decoupled scheme can be then constructed by treating the field

variables in the (Q-weighted) nonlinear terms in (8a) and (8c) explicitly and treating Q implicitly as follows:

$$\sqrt{\rho(\widetilde{\phi}^{j})} \delta_{t}(\sqrt{\rho(\widetilde{\phi}^{j})} \mathbf{u}^{j}) + \nabla P^{j} - \nabla \cdot \left(2\eta(\widetilde{\phi}^{j})\mathbb{D}(\mathbf{u}^{j})\right) 
+ Q^{j} \left(\nabla \cdot \left(\widetilde{\mathbf{u}}^{j} \otimes (\rho(\widetilde{\phi}^{j})\widetilde{\mathbf{u}}^{j} + \widetilde{\mathbf{J}}^{j})\right) - \frac{1}{2}\widetilde{\mathbf{u}}^{j} \nabla \cdot (\rho(\widetilde{\phi}^{j})\widetilde{\mathbf{u}}^{j} + \widetilde{\mathbf{J}}^{j}) + \widetilde{\phi}^{j} \nabla \widetilde{\mu}^{j}\right) = 0, 
\delta_{t} \phi^{j} + Q^{j} \nabla \cdot (\widetilde{\phi}^{j} \widetilde{\mathbf{u}}^{j}) - \nabla \cdot (M(\widetilde{\phi}^{j}) \nabla \mu^{j}) = 0.$$

We can show that the resulting time discretization, which we call the Q-scheme, is a linearly decoupled scheme that is unconditionally energy stable for a slightly different modified energy. While the Q-scheme works reasonably well for the constant mobility case, we observe robustness issues of the Q-scheme when the mobility coefficient is degenerate. In particular, our preliminary numerical experiments with the Q-scheme for a CHNS model with degenerate mobility (the numerical example in Section 3.3) for the rising bubble benchmark problem [41] show that the Q value quickly diminishes to a value close to zero no matter how small the time step size  $\Delta t$  is chosen, which leads to an O(1) constancy error as Q needs to stay around 1 for accuracy of the scheme. This phenomenon is very surprising, which we do not have a good explanation. We will investigate on the issue in more details in our future work.

Finally, we remark that a simple practice to decouple the scheme (11) is to treat the convection term explicitly in equation (11d) by replacing  $\mathbf{u}^j$  by  $\widetilde{\mathbf{u}}^j$ . Due to the explicit convection treatment in (11d), stability is expected to hold under a CFL condition. Although we do not have a rigorous proof of energy stability of this decoupled scheme, ample numerical experiments (not reported here for simplicity) show that taking  $\Delta t = 0.1 h/v_{\text{max}}$  where  $v_{\text{max}}$  is the maximum velocity magnitude is usually enough to obtain a stable simulation.

## 2.3. Spatial discretization

In this subsection, we introduce the classical finite element discretization for the timediscrete system (11) using a mixed finite element method for the velocity and pressure variables and a continuous Galerkin method for the phase-field variables  $\phi$  and  $\mu$ . Due to the Galerkin formulation, it is trivial to show that the energy stability result of Theorem 2.1 naturally carries over to this fully discrete setting.

It is a common practice to introduce stabilized methods for convection-diffusion type problems with a strong convection effect. Here we use the classical SUPG (residual-based) stabilization for the phase-field equation and the SUPG/PSPG/grad-div stabilization for the flow equations; see [38, 7, 37, 39, 5, 2, 40, 15] for more details on stabilized methods.

To this end, let  $\mathcal{T}_h := \{T\}$  be a conforming simplicial triangulation of the domain  $\Omega$ , and let  $\mathcal{E}_h = \{F\}$  be the collection of facets (edges in 2D, faces in 3D) of  $\mathcal{T}_h$ . We set h to be the maximum mesh size of  $\mathcal{T}_h$ . Given a simplex element  $S \subset \mathbb{R}^d$ , d = 1, 2, 3, we denote  $\mathcal{P}^m(S)$  as the space of polynomials of degree at most m on the element S. We denote  $(\cdot, \cdot)_{\Omega}$  as the  $L^2$ -inner product on the domain  $\Omega$ , and  $\|\cdot\|_{\Omega}$  as the  $L^2$ -norm. We introduce the following continuous finite element spaces:

$$X_h^k := \{ w \in H^1(\Omega) : \quad w|_T \in \mathcal{P}^k(T), \quad \forall T \in \mathcal{T}_h \}, \tag{14a}$$

$$\mathbf{Y}_{h}^{k} := \left\{ \mathbf{v} \in [H_{0}^{1}(\Omega)]^{d} : \quad \mathbf{v}|_{T} \in \left\{ \begin{array}{ll} [\mathcal{P}^{1}(T)]^{d} \oplus [\{b_{T}\}]^{d} & \text{if } k = 1, \\ [\mathcal{P}^{k}(T)]^{d} & \text{if } k \geq 2, \end{array} \right. \quad \forall T \in \mathcal{T}_{h} \right\}, \quad (14b)$$

where  $b_T \in \mathcal{P}^d(T)$  is the bubble polynomial that vanishes on the element boundary  $\partial T$ . Note that the velocity and pressure pair  $\mathbf{Y}_h^1 \times X_h^1$  is the mini element [4], while the pair  $\mathbf{Y}_h^k \times X_h^{k-1}$ , for  $k \geq 2$  is the Taylor-Hood element [64].

# 2.3.1. The plain Galerkin method

Given a polynomial degree  $k \geq 1$ , let  $\mathbf{u}_h^0, \phi_h^0, \mu_h^0 \in \mathbf{Y}_h^k \times X_h^k \times X_h^k$  be the interpolation of the initial data  $\mathbf{u}_0, \phi_0$ , and

$$\mu_0 = \frac{\tilde{\sigma}}{\epsilon} (F'(\phi_0) - \epsilon^2 \triangle \phi_0),$$

respectively, and let  $U_h^0$  be given according to the initial data (7b). For any  $j \geq 1$ , the plain Galerkin method finds approximations  $(U_h^j, \mathbf{u}_h^j, P_h^j, \phi_h^j, \mu_h^j) \in \mathbb{R} \times \mathbf{Y}_h^k \times X_h^{k_p} \times X_h^k \times X_h^k$  where  $k_p := \max\{k-1,1\}$  such that

$$\delta_{t}U_{h}^{j} - \frac{1}{2} \left( r(\widetilde{\phi}_{h}^{j}), \delta_{t}\phi_{h}^{j} \right)_{\Omega} = 0, \quad (15a)$$

$$\left( \sqrt{\rho(\widetilde{\phi}_{h}^{j})} \delta_{t} (\sqrt{\rho(\widetilde{\phi}_{h}^{j})} \mathbf{u}_{h}^{j}), \mathbf{v}_{h} \right)_{\Omega} - \left( P_{h}^{j}, \nabla \cdot \mathbf{v}_{h} \right)_{\Omega} + \left( 2\eta(\widetilde{\phi}^{j}) \mathbb{D}(u_{h}^{j}), \mathbb{D}(u_{h}^{j}) \right)_{\Omega}$$

$$- \frac{1}{2} \left( \mathbf{u}_{h}^{j} \otimes (\rho(\widetilde{\phi}_{h}^{j}) \widetilde{\mathbf{u}}_{h}^{j} + \widetilde{\mathbf{J}}_{h}^{j}), \nabla \mathbf{v}_{h} \right)_{\Omega} + \frac{1}{2} \left( \nabla \mathbf{v}_{h} \otimes \left( \rho(\widetilde{\phi}_{h}^{j}) \widetilde{\mathbf{u}}_{h}^{j} + \widetilde{\mathbf{J}}_{h}^{j} \right), \mathbf{u}_{h}^{j} \right)_{\Omega}$$

$$+ \left( \widetilde{\phi}_{h}^{j} \nabla \mu_{h}^{j}, \mathbf{v}_{h} \right)_{\Omega} = (\mathbf{f}, \mathbf{v})_{\Omega}, \quad (15b)$$

$$\left( \nabla \cdot \mathbf{u}_{h}^{j}, q_{h} \right)_{\Omega} = 0, \quad (15c)$$

$$\left( \delta_{t} \phi_{h}^{j}, \xi_{h} \right)_{\Omega} - \left( \widetilde{\phi}_{h}^{j} \mathbf{u}_{h}^{j}, \nabla \xi_{h} \right)_{\Omega} + \left( M(\widetilde{\phi}_{h}^{j}) \nabla \mu_{h}^{j}, \nabla \xi_{h} \right)_{\Omega} = 0, \quad (15d)$$

$$- \frac{\epsilon}{\widetilde{\sigma}} \left( \mu_{h}^{j}, \psi_{h} \right)_{\Omega} + U_{h}^{j} \left( r(\widetilde{\phi}_{h}^{j}), \psi_{h} \right)_{\Omega} + \left( s\phi_{h}^{j}, \psi_{h} \right)_{\Omega} + \epsilon^{2} \left( \nabla \phi_{h}^{j}, \nabla \psi_{h} \right)_{\Omega} = 0, \quad (15e)$$

for all  $(\mathbf{v}_h, q_h, \xi_h, \psi_h) \in \mathbf{Y}_h^k \times X_h^{k_p} \times X_h^k \times X_h^k$ , where

$$\widetilde{\mathbf{J}}_{h}^{j} := \frac{\rho_{1} - \rho_{2}}{2} M(\widetilde{\phi}_{h}^{j}) \nabla \widetilde{\mu}_{h}^{j}. \tag{15f}$$

It is clear from the proof of Theorem 2.1 that the unconditional modified energy stability result of Theorem 2.1 carries over to this fully discrete setting.

#### 2.3.2. The stabilized method

For convection dominated flow problems, it is beneficial to introduce extra stabilization to the plain Galerkin method (15) to suppress numerical oscillations due to strong convection. Here we introduce a classical (residual-based) SUPG-type stabilization for the phase-field equation (15d), and the SUPG/PSPG/grad-div stabilization for the flow

equations (15b)–(15c). More advanced stabilization techniques like the variational multiscale method [5] can also be used. Denoting the following (linearized) residual terms:

$$\mathbf{r}_{u}^{j} := \sqrt{\rho(\widetilde{\phi}_{h}^{j})} \delta_{t}(\sqrt{\rho(\widetilde{\phi}_{h}^{j})} \mathbf{u}_{h}^{j}) + \nabla P_{h}^{j} - \nabla \cdot \left(2\eta(\widetilde{\phi}_{h}^{j}) \mathbb{D}(\mathbf{u}_{h}^{j})\right) + \nabla \cdot \left(\mathbf{u}_{h}^{j} \otimes \left(\rho(\widetilde{\phi}_{h}^{j}) \widetilde{\mathbf{u}}_{h}^{j} + \widetilde{\mathbf{J}}_{h}^{j}\right)\right) - \frac{1}{2} \mathbf{u}_{h}^{j} \nabla \cdot \left(\rho(\widetilde{\phi}_{h}^{j}) \widetilde{\mathbf{u}}_{h}^{j} + \widetilde{\mathbf{J}}_{h}^{j}\right) + \widetilde{\phi}_{h}^{j} \nabla \mu_{h}^{j} - \mathbf{f}_{h}^{j},$$
 (16a)

$$r_p^j := \nabla \cdot \mathbf{u}_p^j,$$
 (16b)

$$r_{\phi}^{j} := \delta_{t} \phi_{h}^{j} + \widetilde{\mathbf{u}}_{h}^{j} \cdot \nabla \phi_{h}^{j} - \nabla \cdot (M(\widetilde{\phi}_{h}^{j}) \nabla \mu_{h}^{j}), \tag{16c}$$

the proposed stabilized method adds to the plain Galerkin method (15) with the following (linear) residual-based stabilization term:

$$B_{s}\left((\mathbf{u}_{h}^{j}, P_{h}^{j}, \phi_{h}^{j}, \mu_{h}^{j}), (\mathbf{v}_{h}, q_{h}, \psi_{h}, \xi_{h})\right) := \sum_{T \in \mathcal{T}_{h}} \int_{T} \tau_{\text{SUPS}}^{j} \left(\widetilde{\mathbf{u}}_{h}^{j} \cdot \nabla \mathbf{v}_{h} + \frac{\nabla q_{h} + \widetilde{\phi}_{h}^{j} \nabla \xi_{h}}{\rho(\widetilde{\phi}_{h}^{j})}\right) \cdot \mathbf{r}_{u}^{j} \, d\mathbf{x}$$

$$+ \sum_{T \in \mathcal{T}_{h}} \int_{T} \rho(\widetilde{\phi}_{h}^{j}) \nu_{\text{LSIC}}^{j} \left(\nabla \cdot \mathbf{v}_{h}\right) \cdot r_{p}^{j} \, d\mathbf{x}$$

$$+ \sum_{T \in \mathcal{T}_{h}} \int_{T} \rho(\widetilde{\phi}_{h}^{j}) \tau_{\text{SUPS}}^{j} \left(\widetilde{\mathbf{u}}_{h}^{j} \cdot \nabla \xi_{h}\right) \cdot r_{\phi}^{j} \, d\mathbf{x}, \qquad (17a)$$

where the stabilization parameters  $\tau_{\text{SUPS}}^{j}$  and  $\nu_{\text{LSIC}}^{j}$  are given by the following formulas, see e.g. [6, Chapter 2] and [43, Chapter 5/8] for discussions on the choice of the stabilization parameters:

$$\tau_{\text{SUPS}} := \left( \frac{4}{(\Delta t^j)^2} + \widetilde{\mathbf{u}}_h^j \cdot \mathbf{G} \widetilde{\mathbf{u}}_h^j + C_I \left( \frac{\eta(\widetilde{\phi}_h^j)}{\rho(\widetilde{\phi}_h^j)} \right)^2 \mathbf{G} : \mathbf{G} \right)^{-1/2}, \tag{17b}$$

$$\nu_{\text{LSIC}} := (\text{tr} \mathbf{G} \, \tau_{\text{SUPS}})^{-1}, \tag{17c}$$

where  $C_I$  is the inverse estimate constant taken to be  $C_I = 3$ , and  $\operatorname{tr} \mathbf{G} = \sum_{i=1}^d \mathbf{G}_{ii}$  is the trace of the element metric tensor  $\mathbf{G} = \mathbf{F}^{-T}\mathbf{F}^{-1}$  with  $\mathbf{F}$  being the element Jacobian matrix. Here we briefly comment on the role of each term on the right hand side of equation (17a). The first term is a stabilization for the momentum equation (8a), which contains the SUPG term, with test function  $\widetilde{\mathbf{U}}_h^j \cdot \nabla \mathbf{v}_h$ , that stabilizes dominating convection, the PSPG term, with test function  $\nabla q_h/\rho(\widetilde{\phi}_h^j)$ , that stabilizes the potential violation of discrete inf-sup condition for the velocity-pressure finite element pair, and the additional stabilization term with test function  $\widetilde{\phi}_h^j \nabla \xi_h/\rho(\widetilde{\phi}_h^j)$  that stabilizes dominated surface tension effects. The second term is the grad-div stabilization term for the mass conservation equation (8b), which gives additional control on the violation of the mass conservation for the velocity-pressure finite element pair. And the last term is the SUPG term for the convective Cahn-Hilliard equation (8c) that again stabilizes dominating convection. Hence, the stabilized

method seeks approximations  $(U_h^j, \mathbf{u}_h^j, P_h^j, \phi_h^j, \mu_h^j) \in \mathbb{R} \times \mathbf{Y}_h^k \times X_h^{k_p} \times X_h^k \times X_h^k$  such that

$$B_g\left((U_h^j, \mathbf{u}_h^j, P_h^j, \phi_h^j, \mu_h^j), (\mathbf{v}_h, q_h, \psi_h, \xi_h)\right) + B_s\left((\mathbf{u}_h^j, P_h^j, \phi_h^j, \mu_h^j), (\mathbf{v}_h, q_h, \psi_h, \xi_h)\right) = (\mathbf{f}^j, \mathbf{v})_{\Omega},$$

$$(18)$$

for all  $(\mathbf{v}_h, q_h, \xi_h, \psi_h) \in \mathbf{Y}_h^k \times X_h^{k_p} \times X_h^k \times X_h^k$ , where  $B_g(\cdot, \cdot)$  is the collection of the left hand side terms in the plain Galerkin method (15). Due to the additional stabilization terms, it is well-known that the velocity/pressure pair for the stabilized method (18) does not need to satisfy the inf-sup condition, and a popular choice is to use equal-order finite element spaces for both quantities; see, e.g., [5]. However, in this work we still stick with the inf-sup stable spaces used for the plain Galerkin method to facilitate a fair comparison between the two methods.

We note particularly that the stabilized method (18) is still a linear scheme. More interestingly, we find that the linear system for the stabilized method is easier to solve than that for the plain Galerkin method (15) due to the effect of the stabilization terms, when a sparse direct solver is used. However, we are not able to establish the same energy stability result in Theorem 2.1 for the stabilized method. We suggest to add the stabilization terms when the flow has a large Reynolds number and/or a large Péclet number. In particular, numerical evidence for the Rayleigh-Taylor instability problem in Section 3.4 below showed that the plain Galerkin method performs surprisingly well for Reynolds number Re = 1000 and Péclet number Pe = 10000, while the stabilized method outperform the plain Galerkin method both in terms of the solution resolution and computational time when the Reynolds number is increased to Re = 5000, where the flow is strongly convection dominated.

## 3. Numerical results

In this section, we present several numerical results for the proposed schemes (15) and (18). In all the simulations, we take  $s = B_0 = 0$  in the SAV model (7b), and use a sparse direct solver to solve the linear system problems. The NGSolve software [58] is used for the simulation.

#### 3.1. Accuracy test

We use the method of manufactured solutions to test the spatial and temporal accuracy of the scheme. In particular, we consider the model (1) with a source term  $f_{\phi}$  in the equation (1c) on a unit square domain, and take the source terms  $f_{\phi}$  and  $\mathbf{f}$  in (1a) such that the exact solution is given as follows:

$$\phi(t, x) = \cos(\pi t) \cos(\pi x) \cos(\pi y),$$

$$\mu(t, x) = \frac{\widetilde{\sigma}}{\epsilon^{-1}} (F'(\phi(t, x)) - \epsilon \triangle \phi(t, x)),$$

$$\mathbf{u}(t, x) = (-\partial_y \Phi(t, x), \partial_x \Phi(t, x))$$

with the stream function  $\Phi(t,x) = \cos(\pi t) (x(1-x)y(1-y))^2$  Furthermore, we take  $\rho_1 = 1$ ,  $\rho_2 = 3$ ,  $\eta_1 = \eta_2 = 0.01$ ,  $\tilde{\sigma} = 0.1$ ,  $\epsilon = 0.1$ , and  $\gamma = 0.01$ . The final time is taken to be T = 0.4, and we use a uniform time step size  $\delta t = h^{(k+1)/2}$  with polynomial degree k = 1 or k = 2. The history of convergence of the  $L^2$ -norm errors in  $\phi_h$ ,  $\mu_h$ , and  $\mathbf{u}_h$  at the final time T = 0.4 on a sequence of uniform square meshes are recorded in Table 1 and Table 2, respectively, for the plain Galerkin method (15) and the stabilized method (18), respectively. For these two tables, we find that the errors for both methods are similar on the same mesh. Moreover, we observe optimal convergence order of k + 1 in the velocity field  $\mathbf{u}_h$  and phase-field variable  $\phi_h$  for both methods. In particular, this indicates the expected second-order temporal accuracy of the proposed temporal discretization.

			$  u-u_h  $		$\ \phi-\phi_h\ $		$\ \mu-\mu_h\ $	
k	1/h	$T/\Delta t$	Error	Order	Error	Order	Error	Order
	10	4	2.734e-02	_	4.940e-03	_	6.328e-04	_
1	20	8	6.622e-03	2.046	7.019e-04	2.815	1.708e-04	1.889
	40	16	1.607e-03	2.043	1.836e-04	1.935	4.386e-05	1.962
	80	32	3.951e-04	2.024	6.088e-05	1.592	1.099e-05	1.996
	10	13	2.477e-03	_	1.793e-04	_	4.325e-05	_
2	20	36	3.102e-04	2.997	3.726e-05	2.267	4.684e-06	3.207
	40	101	3.889e-05	2.996	5.433e-06	2.778	5.573e-07	3.071
	80	286	4.857e-06	3.001	7.555e-07	2.846	6.852e-08	3.024

Table 1: History of convergence of the  $L^2$ -errors for the plain Galerkin method (15).

			$  u-u_h  $		$\ \phi-\phi_h\ $		$\ \mu-\mu_h\ $	
k	1/h	$T/\Delta t$	Error	Order	Error	Order	Error	Order
	10	4	2.727e-02	_	4.940e-03	_	6.841e-04	_
1	20	8	6.616e-03	2.043	6.928e-04	2.834	1.893e-04	1.853
	40	16	1.606e-03	2.042	1.793e-04	1.950	4.708e-05	2.008
	80	32	3.951e-04	2.024	6.035e-05	1.571	1.154e-05	2.029
	10	13	2.473e-03	_	1.684e-04	_	5.425 e-05	_
2	20	36	3.100e-04	2.996	3.697e-05	2.188	5.497e-06	3.303
	40	101	3.889e-05	2.995	5.428e-06	2.768	5.913e-07	3.217
	80	286	4.858e-06	3.001	7.555e-07	2.845	6.985e-08	3.081

Table 2: History of convergence of the  $L^2$ -errors for the stabilized method (18).

## 3.2. Energy stability test

In this example, we confirm numerically the energy stability result in Theorem 2.1 for the plain Galerkin method (15). We use the same modeling parameters as in the previous example, but ignore the source terms  $\mathbf{f}$  and  $f_{\phi}$  therein. The initial condition is taken to be

$$\phi_0(x, y) = \cos(4\pi x)\cos(4\pi y),$$
  

$$\mathbf{u}_0(x, y) = (-\partial_y \Phi_0(x, y), \partial_x \Phi_0(x, y)),$$

with  $\Phi_0(x,y) = 16 (x(1-x)y(1-y))^2$  We take final time T=40. The plain Galerkin method (15) on a uniform triangular mesh with mesh size h=0.05 and uniform time stepping with time step size  $\Delta t = 0.05$  is used for the simulation.

For this problem, Theorem 2.1 indicates that following (modified) energy stability result for the numerical results of our method:

$$\widetilde{E}_h^j - \widetilde{E}_h^{j-1} \le -\Delta t \operatorname{Diss}_h^j$$

where

$$\begin{split} \widetilde{E}_h^j := & \frac{1}{4} \left\| \sqrt{\rho(\widetilde{\phi}_h^j)} \mathbf{u}_h^j \right\|_{\Omega}^2 + \frac{1}{4} \left\| 2 \sqrt{\rho(\widetilde{\phi}_h^j)} \mathbf{u}_h^j - \sqrt{\rho(\widetilde{\phi}_h^{j-1})} \mathbf{u}_h^{j-1} \right\|_{\Omega}^2 \\ & + \frac{1}{4} \widetilde{\sigma} \epsilon \| \nabla \phi_h^j \|_{\Omega}^2 + \frac{1}{4} \widetilde{\sigma} \epsilon \| \nabla (2 \phi_h^j - \phi_h^{j-1}) \|_{\Omega}^2 + \frac{\widetilde{\sigma}}{2\epsilon} \left( (U_h^j)^2 + (2 U_h^j - U_h^{j-1})^2 \right) \end{split}$$

is the modified total energy, and

$$\operatorname{Diss}_{h}^{j} := \left\| \sqrt{2\eta(\widetilde{\phi}_{h}^{j})} \mathbf{D} \mathbf{u}_{h}^{j} \right\|_{\Omega}^{2} + \left\| \sqrt{M(\widetilde{\phi}_{h}^{j})} \nabla \mu_{h}^{j} \right\|_{\Omega}^{2}$$

is the physical dissipation rate at time  $t^{j}$ . The above result is numerically confirmed in Figure 1, where we plot the evolution of the modified energy along with the true energy

$$\begin{split} E_h^j := & \frac{1}{4} \left\| \sqrt{\rho(\widetilde{\phi}_h^j)} \mathbf{u}_h^j \right\|_{\Omega}^2 + \frac{1}{4} \left\| 2 \sqrt{\rho(\widetilde{\phi}_h^j)} \mathbf{u}_h^j - \sqrt{\rho(\widetilde{\phi}_h^{j-1})} \mathbf{u}_h^{j-1} \right\|_{\Omega}^2 \\ & + \frac{1}{4} \widetilde{\sigma} \epsilon \| \nabla \phi_h^j \|_{\Omega}^2 + \frac{1}{4} \widetilde{\sigma} \epsilon \| \nabla (2\phi_h^j - \phi_h^{j-1}) \|_{\Omega}^2 + \frac{\widetilde{\sigma}}{2\epsilon} \int_{\Omega} (F(\phi_h^j) + F(2\phi_h^j - \phi_h^{j-1})) \, \mathrm{d}\mathbf{x} \end{split}$$

and the evolution of the dissipation rates. In particular, from Figure 1 we observe that that the modified total energy  $\widetilde{E}_h$  and the true energy  $E_h$  are on top of each other, and the dissipation rates  $\frac{\widetilde{E}_h^{j-1}-\widetilde{E}_h^j}{\Delta t}$  and  $\mathrm{Diss}_h^j$  are on top of each other.

#### 3.3. Rising bubble

We consider the rising bubble benchmark problem proposed in [41]. The test setup is extensively described in [41]. The domain  $[0,1] \times [0,2]$  is filled with fluid 1 ( $\phi \approx 1$ ) except for a circular bubble, which consists of fluid 2 ( $\phi \approx -1$ ). The initial bubble has a radius of 0.25 with its center at (0.5, 0.5). The gravitational source term  $\mathbf{f} = \rho(0, -0.98)$  is used in the momentum equation (8a). Following [41], we consider the following two test cases:

Case 1: 
$$\rho_1 = 100, \rho_2 = 1000, \eta_1 = 1, \eta_2 = 10, \sigma = 24.5,$$

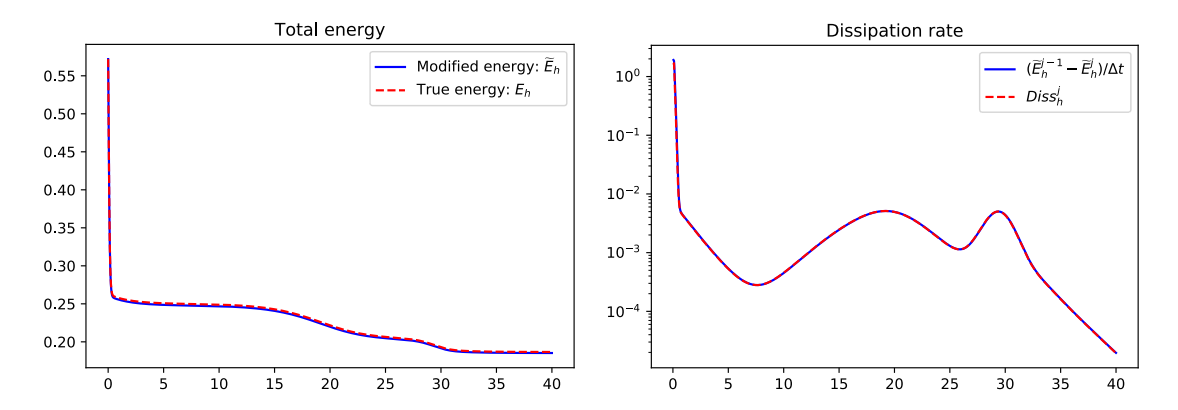


Figure 1: Evolution of energies and dissipation rates for the plain Galerkin method (15) on a uniform triangular mesh with mesh size h = 0.05 and uniform time step size  $\Delta t = 0.05$ . (For interpretation of the colors in this figure, the reader is referred to the web version of this article.)

Case 2: 
$$\rho_1 = 1, \rho_2 = 1000, \eta_1 = 0.1, \eta_2 = 10, \sigma = 1.96.$$

We take the final time of simulation to be t = 3. For Case 1, the bubble reaches a stable bubble ellipsoidal shape; for Case 2, it develops a more non-convex shape and thin filaments, which may or may not break, due to a decreased surface tension and larger density ratio [41].

Due to symmetry of the problem, we run the simulation only on the half domain  $\Omega = [0, 0.5] \times [0, 2]$ . As for the boundary conditions, we use a homogeneous Neumann boundary condition (2b) for the phase-field variables  $\phi$  and  $\mu$ , and no slip velocity boundary condition on the horizontal boundaries and free slip velocity boundary condition on the vertical boundaries. We take the interface thickness  $\epsilon$  to be either 0.01 or 0.005. Based on preliminary numerical experiments, it was observed that taking the mobility coefficient  $\gamma \in \left(\frac{\epsilon}{20\sigma}, \frac{\epsilon}{5\sigma}\right)$  in (1f) leads to a fairly good agreement of our simulation results with reference data provided in [41]. We use  $\gamma = \frac{\epsilon}{10\sigma}$  for our simulation results reported in this subsection. Furthermore, the initial condition for  $\phi$  is taken to be a hyperbolic tangent:

$$\phi_0(x,y) = \tanh\left(\frac{r - 0.25}{\sqrt{2}\epsilon}\right), \quad r = \sqrt{(x - 0.5)^2 + (y - 0.5)^2},$$

while the initial condition for velocity is zero.

For each  $\epsilon$ , we consider a triangular mesh that is locally refined on the sub-region  $\Omega_1 := [0.15, 0.5] \times [0.2 \times 1.4]$ , where the mesh size is  $h = 1.6\epsilon$  on  $\Omega_1$  and  $h = 6.4\epsilon$  on  $\Omega \setminus \Omega_1$ , see an illustration in Figure 2. We apply the plain Galerkin method (15) with polynomial degree k = 2 on these meshes and take uniform time step size  $\Delta t = 4 \times 10^{-3}$  or  $\Delta t = 2 \times 10^{-3}$  when  $\epsilon = 0.01$ , and  $\Delta t = 2 \times 10^{-3}$  or  $\Delta t = 1 \times 10^{-3}$  when  $\epsilon = 0.005$ . Contour plots of the phase field variable  $\phi_h$  for the two cases at final time t = 3 using  $\epsilon = 0.005$  and  $\Delta t = 1 \times 10^{-3}$  are shown in Figure 2 (c) and (d). We observe the expected stable ellipsoidal bubble for Case 1, and the non-convex shape with filaments for Case 2. In particular, our simulation results in a break of the bubble filaments for Case 2.

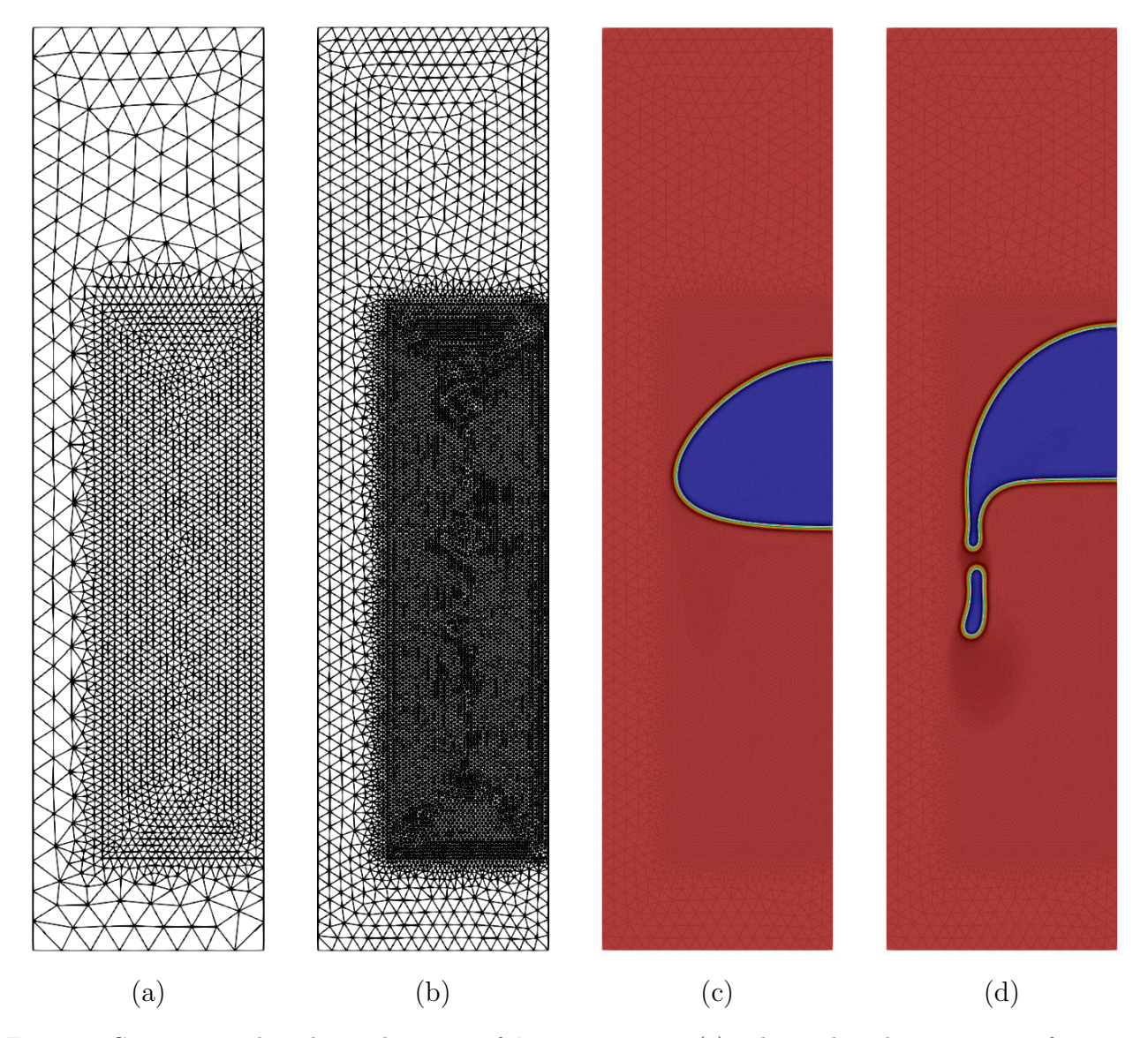


Figure 2: Computational meshes and contour of  $\phi_h$  at time t=3. (a): The mesh with 2278 vertices for  $\epsilon=0.01$ . (b): The mesh with 8442 vertices for  $\epsilon=0.005$ . (c) Contour of  $\phi_h$  at t=3 for Case 1 using  $\epsilon=0.005$  and  $\Delta t=0.002$  (red color:  $\phi=1$ , blue color:  $\phi=-1$ ). (d) Contour of  $\phi_h$  at t=3 for Case 2 using  $\epsilon=0.005$  and  $\Delta t=0.002$ . (For interpretation of the colors in this figure, the reader is referred to the web version of this article.)

We compute the following three benchmark quantities and compare them with reference values from group 3 in [41], which solves the sharp interface model using an arbitrary Euler-Lagrangian finite element method within the MooNMD software [44]:

# • Center of mass

$$y_c = \frac{\int_{\phi < 0} y \, \mathrm{dx}}{\int_{\phi < 0} 1 \, \mathrm{dx}},$$

where y is the vertical coordinate.

• Circularity:

$$c = \frac{\text{perimeter of area-equivalent circle}}{\text{perimeter of bubble}} = \frac{2\sqrt{\int_{\phi<0}\pi\,\mathrm{dx}}}{\int_{\phi=0}1\,\mathrm{ds}}.$$

• Rise velocity:

$$V_c = \frac{\int_{\phi < 0} v \, \mathrm{dx}}{\int_{\phi < 0} 1 \, \mathrm{dx}}$$

where v is the vertical component of the velocity  $\mathbf{u}$ .

Figure 3 shows the evolution of these benchmark quantities over time for Case 1. We observe an excellent agreement with reference data for the center of mass and rising velocity for all four simulation results. We also have a very good agreement with reference data for the circularity, where an improved agreement is observed for t > 1.5 when we decrease interface thickness  $\epsilon$  from 0.01 to 0.005.

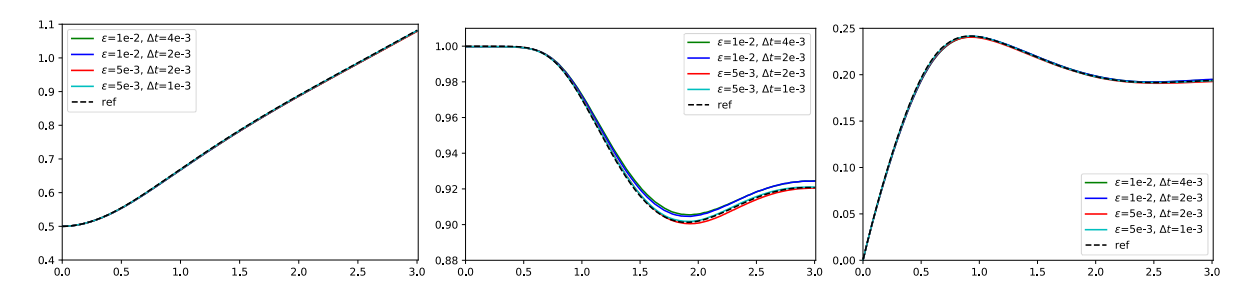


Figure 3: Center of mass (left), circularity (middle), and rising velocity (right) over time for Case 1. Reference data is taken from group 3 of [41]. (For interpretation of the colors in this figure, the reader is referred to the web version of this article.)

Figure 4 shows the evolution of these benchmark quantities over time for Case 2. We observe an excellent agreement with the reference data for all the three quantities up to time t = 1.5. The results for the center of mass for  $t \in [1.5, 3]$  also matches well with the reference data. Meanwhile, we observe a better match of the circularity with the reference data for  $t \in [1.5, 3]$  when decreasing  $\epsilon$  from 0.01 to 0.005. Finally, for the rising velocity, we observe a better match with the reference data for  $t \in [1.5, 2]$  when decreasing  $\epsilon$  from 0.01 to 0.005.

## 3.4. Rayleigh-Taylor instability

The Rayleigh-Taylor instability is a two-phase instability which occurs whenever two fluids of different density are accelerated against each other. We consider a similar setting as in [29]. This problem consists of two layers of fluid initially at rest in the gravity field in the domain  $\Omega = [0, 1/2] \times [-2, 2]$ . The initial position of the perturbed interface is  $\eta(x) = -0.1\cos(2\pi x)$ . The heavy fluid is above and the density ratio is 3 ( $\rho_1 = 1$ ,  $\rho_2 = 3$ ). The viscosity in both fluids is taken to be  $\eta_1 = \eta_2 = \sqrt{2}/Re$ , where Re is

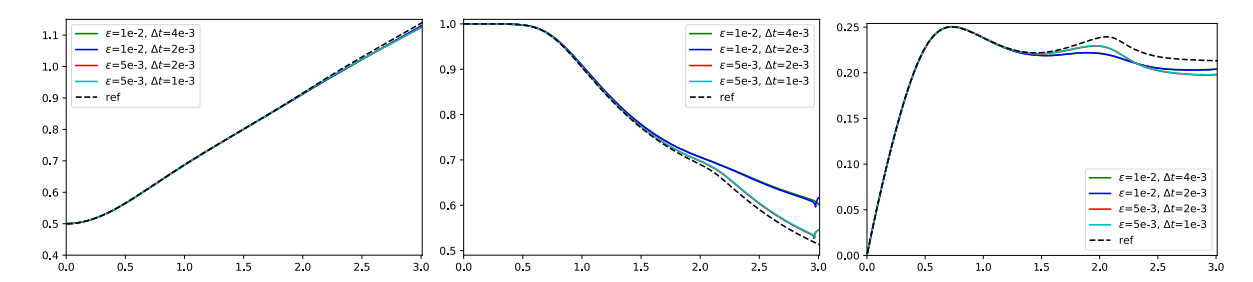


Figure 4: Center of mass (left), circularity (middle), and rising velocity (right) over time for Case 2. Reference data is taken from group 3 of [41]. (For interpretation of the colors in this figure, the reader is referred to the web version of this article.)

the Reynolds number. The (initial) transition between the two fluids is regularized by hyperbolic tangent:

$$\phi(t=0) = \tanh\left(\frac{1}{\sqrt{2\epsilon}}(y+0.1\cos(2\pi x))\right).$$

We consider the gravitational source term  $\mathbf{f} = \rho(0, -g)$  with g = 2. The other modeling parameters are given as follows:

$$\tilde{\sigma} = 10^{-4}, \ Re \in \{1000, 5000\}, \ \epsilon \in \{0.01, 0.005\}, \ \gamma = \epsilon.$$

The final time of simulation is t=2.5. We note that the Reynolds number is defined as  $Re = \rho_1 U d/\eta_1$  which varies according to the viscosity  $\eta_1 = \sqrt{2}/Re$ , cf. [29], with the characteristic velocity  $U = d^{1/2}/g^{1/2}$ . Note also the diffusional Peclet number  $Pe = \frac{\rho_1 U d}{\gamma \tilde{\sigma}} = \frac{\sqrt{2} \times 10^4}{\epsilon}$ , cf. [55]. Hence this numerical experiment is set up in the advection dominated regime.

For each  $\epsilon$ , we consider a triangular mesh that is locally refined on the sub-region  $\Omega_1 := [0, 0.5] \times [-1.25 \times 0.75]$ , where the mesh size is  $h_0 = 1.6\epsilon$  on  $\Omega_1$  and is  $4h_0$  on  $\Omega \setminus \Omega_1$ , see an illustration in Figure 5. For the case with Re = 1000, we apply the plain Galerkin method (15) with polynomial degree k=2 and take a variable time step size  $\Delta t^n = cfl \, h_0/v_{\rm max}^n$  with the CFL number cfl = 0.1, where  $v_{\rm max}^n$  is the estimated maximum velocity magnitude at time  $t^n$ . For the case with Re = 5000, we apply both the plain Galerkin method (15) and the stabilized method (18) with polynomial degree k=2, and take a variable time step size  $\Delta t^n = cfl h_0/v_{\rm max}^n$ , where we reduce the CFL number to be cfl = 0.05. We note that for the case with Re = 5000, using cfl = 0.1 leads to low quality solutions with large numerical oscillations for both methods. We mention that the locally refined mesh is about half the size of a uniformly refined mesh with mesh size  $h = h_0$ , and the total number of time steps is also about half of a uniform time stepping with step size  $\Delta t = cf l h_0 / v_{\text{max}}$  where  $v_{\text{max}} \approx 2.5$  is the estimated maximum velocity magnitude for all time  $t \in [0, 2.5]$ . The quality of numerical results for each scheme on the locally refined mesh with variable time stepping is observed to be qualitatively similar to the same method on a uniform mesh with mesh size  $h_0$  and uniform time stepping  $\Delta t = cfl h_0/v_{\text{max}}$ , with the former being at least 25% cheaper to computer.

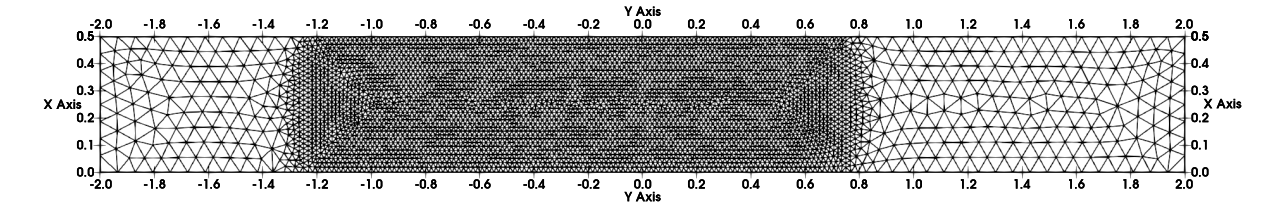


Figure 5: (90-degree rotated) computational mesh for  $\epsilon = 0.01$  (4658 triangular elements).

The time evolution of the contour of the phase-field variable  $\phi_h$  for Re = 1000 (for the plain Galerkin method) is plotted in Figure 6 at times 1, 1.5, 1.75, 2, 2.25, 2.5. We observe that the solutions on the two meshes are consistent in that they show similar structures and differ only in fine details at large time. In particular, no visible numerical oscillation is observed for this case.

The time evolutions of the contour of the phase-field variable  $\phi_h$  for Re=5000 for both methods for  $\epsilon=0.01$  on the coarse mesh and for  $\epsilon=0.005$  on the fine mesh, respectively, are plotted in Figure 7, and Figure 8, respectively. From these figures, we observe that (1) both the plain Galerkin method and the stabilized method produce qualitatively similar results on the same mesh, (2) the solution for the plain Galerkin method show visible numerical oscillations (the shaded area) near the two-phase interface especially on the coarse mesh in the top row of Figure 7, while no visible numerical oscillations are observed the stabilized method, (3) the solutions on the two meshes for both schemes are consistent in that they show similar structures and differ only in fine details at large time and consist in the development of structures within the main vortex that are more complex on the fine mesh than on the coarse one. Moreover, we point out that the computational cost of the sparse direct linear system solver per time step is about 12 seconds for the plain Galerkin method , and about 7.4 seconds for the stabilized method on the fine mesh. Hence, the stabilized method outperform the plain Galerkin method both in terms of solution quality and computational cost in this case.

Finally, we note that all these results are qualitatively similar to the results in [29], where a stabilized projection FEM was used to solve the variable density flow without surface tension effects.

#### 4. Conclusion and discussions

In this article we propose a second—order BDF time-stepping method of variable time step size combined with the SUPG/PSPG/grad-div stabilized finite elements for solving an incompressible two-phase flow model of variable densities in the advection dominated regime. We show that the scheme preserves the underlying energy law of the model when uniform time step size is utilized without additional stabilization. Numerical results confirm the accuracy and stability of the scheme. Moreover, the benchmark of Rayleigh-Taylor instability in the advection dominated regime demonstrate that our scheme well captures the details of the instability.

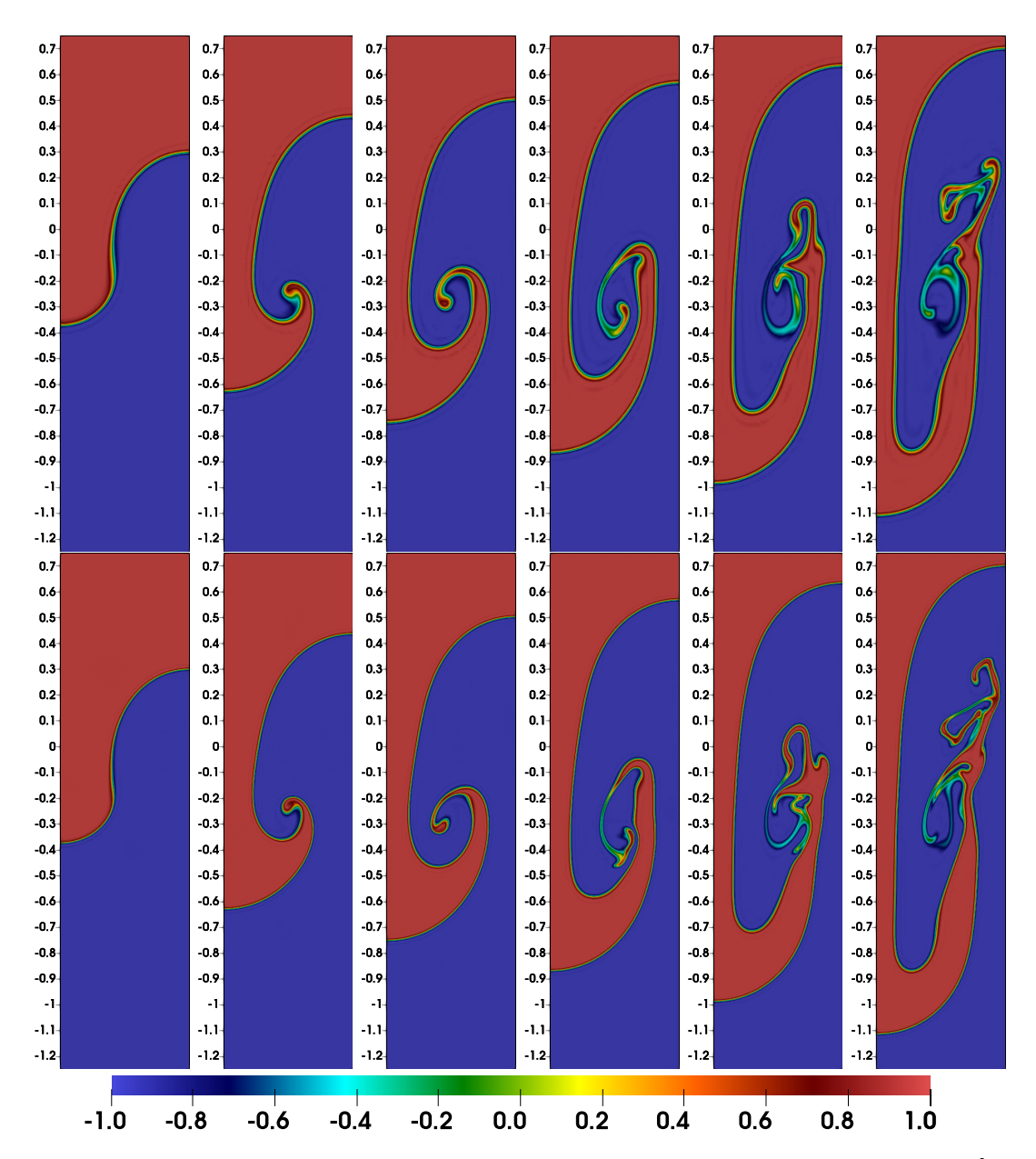


Figure 6: Re = 1000. Contour of the Rayleigh-Taylor instability problem on the subdomain  $[0, 0.5] \times [-1.25, 0.75]$  at time t = 1, 1.5, 1.75, 2.0, 2.25, 2.5 (from left to right) for the plain Galerkin method (15) with polynomial degree k = 2. Top:  $\epsilon = 0.01$  on a triangular mesh with 4658 elements. Bottom:  $\epsilon = 0.005$  on a triangular mesh with 18560 elements. (For interpretation of the colors in this figure, the reader is referred to the web version of this article.)

In spite of the efficiency and unconditional stability of the SAV-based decoupled numerical schemes in the diffusion dominated regime (see Remark 2.3), these methods do not seem to perform well in the advection dominated regime with a degenerate mobility function. This issue warrants further investigation.

In future work, we would like to develop an unconditionally energy stable divergencefree hybridizable discontinuous Galerkin scheme for solving the phase field model (1) where the velocity approximation is solenoidal for all time, by combining the proposed

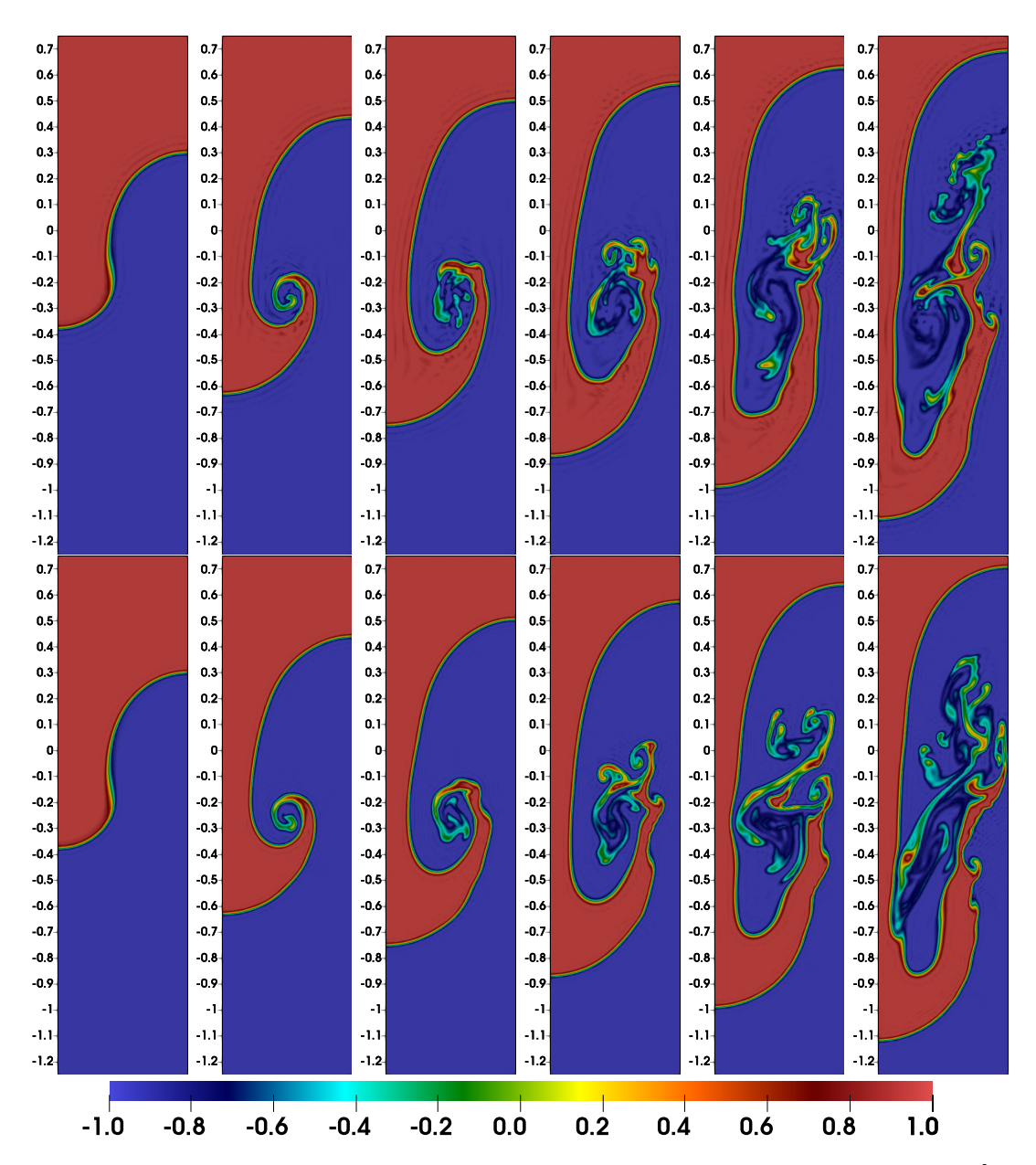


Figure 7: Re = 5000. Contour of the Rayleigh-Taylor instability problem on the subdomain  $[0, 0.5] \times [-1.25, 0.75]$  at time t = 1, 1.5, 1.75, 2.0, 2.25, 2.5 (from left to right). for  $\epsilon = 0.01$  on a triangular mesh with 4658 elements. Top row: the plain Galerkin method (15) with polynomial degree k = 2. Bottom row: the stabilized method (18) with polynomial degree k = 2. (For interpretation of the colors in this figure, the reader is referred to the web version of this article.)

temporal discretization in this work and the spatial discretization in [24].

# Acknowledgements

G. Fu acknowledge the partial support of this work from U.S. National Science Foundation through grant DMS-2012031. D. Han is supported by the U.S. National Science Foundation via DMS-1912715.

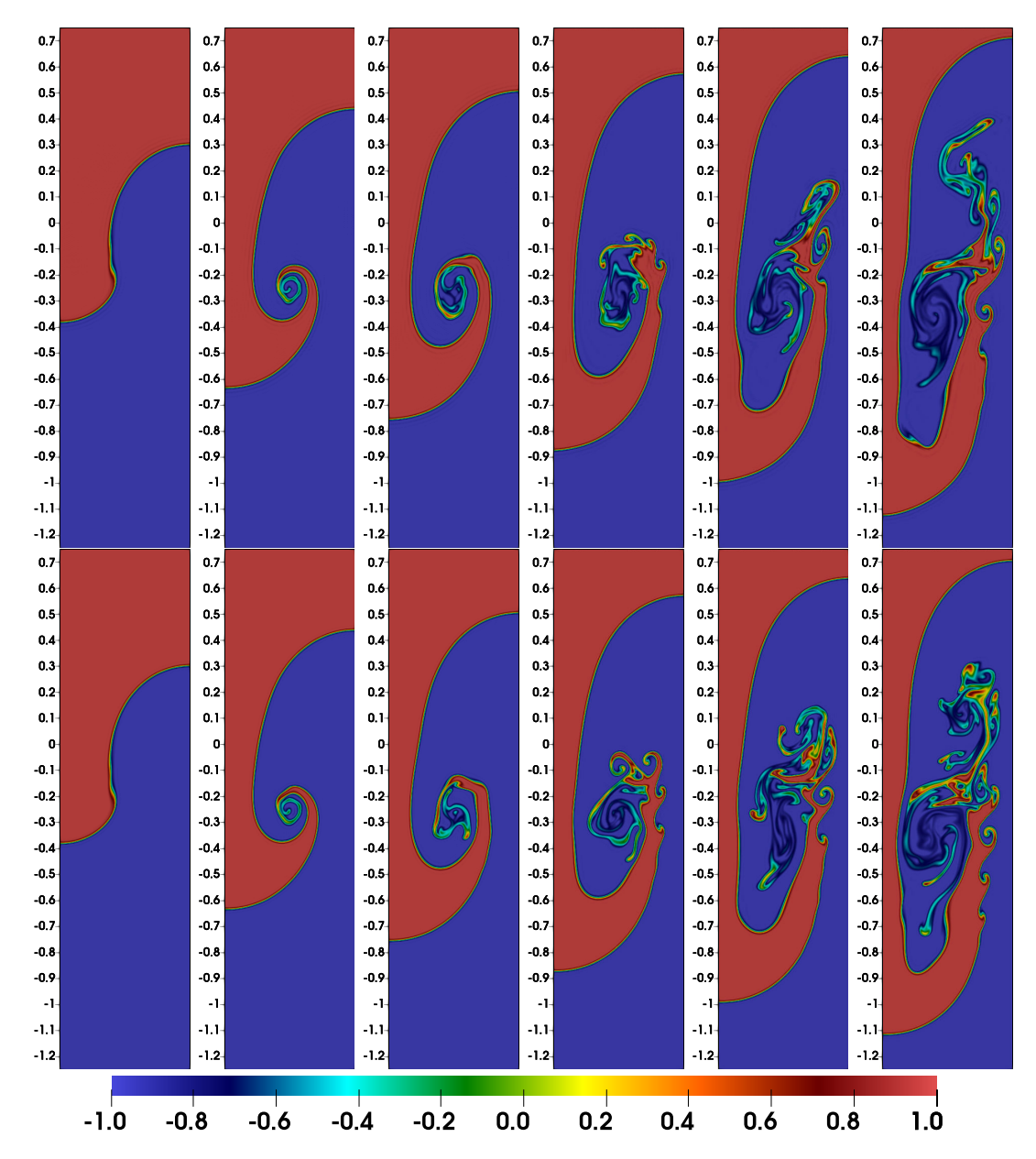


Figure 8: Re = 5000. Contour of the Rayleigh-Taylor instability problem on the subdomain  $[0, 0.5] \times [-1.25, 0.75]$  at time t = 1, 1.5, 1.75, 2.0, 2.25, 2.5 (from left to right) for  $\epsilon = 0.005$  on a triangular mesh with 18560 elements. Top row: the plain Galerkin method (15) with polynomial degree k = 2. Bottom row: the stabilized method (18) with polynomial degree k = 2. (For interpretation of the colors in this figure, the reader is referred to the web version of this article.)

# References

- [1] Helmut Abels, Harald Garcke, and Günther Grün. Thermodynamically consistent, frame indifferent diffuse interface models for incompressible two-phase flows with different densities. *Math. Models Methods Appl. Sci.*, 22(3):1150013, 40, 2012.
- [2] N. Ahmed, T. Chacón R., V. John, and S. Rubino. A review of variational multiscale

- methods for the simulation of turbulent incompressible flows. Arch. Comput. Methods Eng., 24(1):115–164, 2017.
- [3] D. M. Anderson, G. B. McFadden, and A. A. Wheeler. Diffuse-interface methods in fluid mechanics. In *Annual review of fluid mechanics*, *Vol. 30*, volume 30 of *Annu. Rev. Fluid Mech.*, pages 139–165. Annual Reviews, Palo Alto, CA, 1998.
- [4] D. N. Arnold, F. Brezzi, and M. Fortin. A stable finite element for the Stokes equations. *Calcolo*, 21(4):337–344 (1985), 1984.
- [5] Y. Bazilevs, V. M. Calo, J. A. Cottrell, T. J. R. Hughes, A. Reali, and G. Scovazzi. Variational multiscale residual-based turbulence modeling for large eddy simulation of incompressible flows. *Comput. Methods Appl. Mech. Engrg.*, 197(1-4):173–201, 2007.
- [6] Y. Bazilevs, K. Takizawa, and T. E. Tezduyar. Computational Fluid-Structure Interaction: Methods and Applications. John Wiley & Sons, Ltd, 2013.
- [7] A. N. Brooks and T. J. R. Hughes. Streamline upwind/Petrov-Galerkin formulations for convection dominated flows with particular emphasis on the incompressible Navier-Stokes equations. Comput. Methods Appl. Mech. Engrg., 32(1-3):199–259, 1982. FENOMECH "81, Part I (Stuttgart, 1981).
- [8] Hector D. Ceniceros and Carlos J. García-Cervera. A new approach for the numerical solution of diffusion equations with variable and degenerate mobility. *J. Comput. Phys.*, 246:1–10, 2013.
- [9] Wenbin Chen, Wenqiang Feng, Yuan Liu, Cheng Wang, and Steven M. Wise. A second order energy stable scheme for the Cahn-Hilliard-Hele-Shaw equations. *Discrete Contin. Dyn. Syst. Ser. B*, 24(1):149–182, 2019.
- [10] Wenbin Chen, Yuan Liu, Cheng Wang, and Steven M. Wise. Convergence analysis of a fully discrete finite difference scheme for the Cahn-Hilliard-Hele-Shaw equation. *Math. Comp.*, 85(301):2231–2257, 2016.
- [11] Wenbin Chen, Xiaoming Wang, Yue Yan, and Zhuying Zhang. A second order BDF numerical scheme with variable steps for the Cahn-Hilliard equation. SIAM J. Numer. Anal., 57(1):495–525, 2019.
- [12] Kelong Cheng, Wenqiang Feng, Cheng Wang, and Steven M. Wise. An energy stable fourth order finite difference scheme for the Cahn-Hilliard equation. *J. Comput. Appl. Math.*, 362:574–595, 2019.

- [13] Kelong Cheng, Cheng Wang, and Steven M. Wise. An energy stable BDF2 Fourier pseudo-spectral numerical scheme for the square phase field crystal equation. *Commun. Comput. Phys.*, 26(5):1335–1364, 2019.
- [14] Xinyu Cheng, Dong Li, Keith Promislow, and Brian Wetton. Asymptotic behaviour of time stepping methods for phase field models. *J. Sci. Comput.*, 86(3):Paper No. 32, 34, 2021.
- [15] R. Codina, S. Badia, J. Baiges, and J. Principe. Variational Multiscale Methods in Computational Fluid Dynamics. In E. Stein, R. De Borst, and T. J. R. Hughes, editors, *Encyclopedia of Computational Mechanics Second Edition, Part 1 Fluids*. John Wiley & Sons, 2018.
- [16] Shibin Dai and Qiang Du. Coarsening mechanism for systems governed by the Cahn-Hilliard equation with degenerate diffusion mobility. *Multiscale Model. Simul.*, 12(4):1870–1889, 2014.
- [17] Shibin Dai and Qiang Du. Weak solutions for the Cahn-Hilliard equation with degenerate mobility. *Arch. Ration. Mech. Anal.*, 219(3):1161–1184, 2016.
- [18] Amanda E. Diegel, Xiaobing H. Feng, and Steven M. Wise. Analysis of a mixed finite element method for a Cahn-Hilliard-Darcy-Stokes system. *SIAM J. Numer. Anal.*, 53(1):127–152, 2015.
- [19] Amanda E. Diegel, Cheng Wang, Xiaoming Wang, and Steven M. Wise. Convergence analysis and error estimates for a second order accurate finite element method for the Cahn-Hilliard-Navier-Stokes system. *Numer. Math.*, 137(3):495–534, 2017.
- [20] C. M. Elliott and A. M. Stuart. The global dynamics of discrete semilinear parabolic equations. SIAM J. Numer. Anal., 30(6):1622–1663, 1993.
- [21] David J. Eyre. Unconditionally gradient stable time marching the Cahn-Hilliard equation. In Computational and mathematical models of microstructural evolution (San Francisco, CA, 1998), volume 529 of Mater. Res. Soc. Sympos. Proc., pages 39–46. MRS, Warrendale, PA, 1998.
- [22] Wenqiang Feng, Cheng Wang, Steven M. Wise, and Zhengru Zhang. A second-order energy stable backward differentiation formula method for the epitaxial thin film equation with slope selection. *Numer. Methods Partial Differential Equations*, 34(6):1975–2007, 2018.
- [23] Xiaobing Feng and Steven Wise. Analysis of a Darcy-Cahn-Hilliard diffuse interface model for the Hele-Shaw flow and its fully discrete finite element approximation. SIAM J. Numer. Anal., 50(3):1320–1343, 2012.

- [24] Guosheng Fu. A divergence-free HDG scheme for the Cahn-Hilliard phase-field model for two-phase incompressible flow. *J. Comput. Phys.*, 419:109671, 16, 2020.
- [25] Karl Glasner and Saulo Orizaga. Improving the accuracy of convexity splitting methods for gradient flow equations. *J. Comput. Phys.*, 315:52–64, 2016.
- [26] Yuezheng Gong, Jia Zhao, and Qi Wang. Arbitrarily high-order linear energy stable schemes for gradient flow models. *J. Comput. Phys.*, 419:109610, 20, 2020.
- [27] Yuezheng Gong, Jia Zhao, Xiaogang Yang, and Qi Wang. Fully discrete second-order linear schemes for hydrodynamic phase field models of binary viscous fluid flows with variable densities. SIAM J. Sci. Comput., 40(1):B138–B167, 2018.
- [28] J.-L. Guermond and L. Quartapelle. A projection FEM for variable density incompressible flows. *J. Comput. Phys.*, 165(1):167–188, 2000.
- [29] J.-L. Guermond and L. Quartapelle. A projection FEM for variable density incompressible flows. *J. Comput. Phys.*, 165(1):167–188, 2000.
- [30] F. Guillén-González and G. Tierra. On linear schemes for a Cahn-Hilliard diffuse interface model. J. Comput. Phys., 234:140–171, 2013.
- [31] Francisco Guillén-González and Giordano Tierra. Splitting schemes for a Navier-Stokes-Cahn-Hilliard model for two fluids with different densities. *J. Comput. Math.*, 32(6):643–664, 2014.
- [32] Z. Guo, P. Lin, J. Lowengrub, and S. M. Wise. Mass conservative and energy stable finite difference methods for the quasi-incompressible Navier-Stokes-Cahn-Hilliard system: primitive variable and projection-type schemes. *Comput. Methods Appl. Mech. Engrg.*, 326:144–174, 2017.
- [33] Daozhi Han. A decoupled unconditionally stable numerical scheme for the Cahn-Hilliard-Hele-Shaw system. J. Sci. Comput., 66(3):1102–1121, 2016.
- [34] Daozhi Han and Xiaoming Wang. A second order in time, uniquely solvable, unconditionally stable numerical scheme for Cahn–Hilliard–Navier–Stokes equation. *J. Comput. Phys.*, 290:139–156, 2015.
- [35] Yonghong Hao, Qiumei Huang, and Cheng Wang. A third order BDF energy stable linear scheme for the no-slope-selection thin film model. *Commun. Comput. Phys.*, 29(3):905–929, 2021.
- [36] Qiaolin He, Roland Glowinski, and Xiao-Ping Wang. A least-squares/finite element method for the numerical solution of the Navier-Stokes-Cahn-Hilliard system modeling the motion of the contact line. *J. Comput. Phys.*, 230(12):4991–5009, 2011.

- [37] T. J. R. Hughes. Multiscale phenomena: Green's functions, the Dirichlet-to-Neumann formulation, subgrid scale models, bubbles and the origins of stabilized methods. *Comput. Methods Appl. Mech. Engrg.*, 127(1-4):387–401, 1995.
- [38] T. J. R. Hughes and A. Brooks. A multidimensional upwind scheme with no crosswind diffusion. In Finite element methods for convection dominated flows (Papers, Winter Ann. Meeting Amer. Soc. Mech. Engrs., New York, 1979), volume 34 of AMD, pages 19–35. Amer. Soc. Mech. Engrs. (ASME), New York, 1979.
- [39] T. J. R. Hughes, G. R. Feijóo, L. Mazzei, and J.-B. Quincy. The variational multiscale method—a paradigm for computational mechanics. *Comput. Methods Appl. Mech. Engrg.*, 166(1-2):3–24, 1998.
- [40] T. J. R. Hughes, G. Scovazzi, and L. P. Franca. Multiscale and Stabilized Methods. In E. Stein, R. De Borst, and T. J. R. Hughes, editors, *Encyclopedia of Computational Mechanics Second Edition*, Part 1 Fluids. John Wiley & Sons, 2018.
- [41] S. Hysing, S. Turek, D. Kuzmin, N. Parolini, E. Burman, S. Ganesan, and L. Tobiska. Quantitative benchmark computations of two-dimensional bubble dynamics. *Internat. J. Numer. Methods Fluids*, 60(11):1259–1288, 2009.
- [42] Jie Jiang, Yinghua Li, and Chun Liu. Two-phase incompressible flows with variable density: an energetic variational approach. *Discrete Contin. Dyn. Syst.*, 37(6):3243–3284, 2017.
- [43] V. John. Finite element methods for incompressible flow problems, volume 51 of Springer Series in Computational Mathematics. Springer, Cham, 2016.
- [44] V. John and G. Matthies. MooNMD—a program package based on mapped finite element methods. *Comput. Vis. Sci.*, 6(2-3):163–169, 2004.
- [45] V. V. Khatavkar, P. D. Anderson, P. C. Duineveld, and H. E. H. Meijer. Diffuse-interface modelling of droplet impact. *J. Fluid Mech.*, 581:97–127, 2007.
- [46] Junseok Kim, Kyungkeun Kang, and John Lowengrub. Conservative multigrid methods for Cahn-Hilliard fluids. *J. Comput. Phys.*, 193(2):511–543, 2004.
- [47] Andrea G. Lamorgese, Dafne Molin, and Roberto Mauri. Phase field approach to multiphase flow modeling. *Milan J. Math.*, 79(2):597–642, 2011.
- [48] Alpha Albert Lee, Andreas Münch, and Endre Süli. Sharp-interface limits of the Cahn-Hilliard equation with degenerate mobility. SIAM J. Appl. Math., 76(2):433–456, 2016.

- [49] Shen Jie Li, Xiaoli and Zhengguang Liu. New sav-pressure correction methods for the navier-stokes equations: Stability and error analysis. *Math. Comp.*, 2021.
- [50] X. Li and J. Shen. On a SAV-MAC scheme for the Cahn-Hilliard-Navier-Stokes phase-field model and its error analysis for the corresponding Cahn-Hilliard-Stokes case. *Math. Models Methods Appl. Sci.*, 30(12):2263–2297, 2020.
- [51] Yibao Li, Yongho Choi, and Junseok Kim. Computationally efficient adaptive time step method for the Cahn-Hilliard equation. *Comput. Math. Appl.*, 73(8):1855–1864, 2017.
- [52] Hong-lin Liao, Tao Tang, and Tao Zhou. A second-order and nonuniform time-stepping maximum-principle preserving scheme for time-fractional Allen-Cahn equations. *J. Comput. Phys.*, 414:109473, 16, 2020.
- [53] Lianlei Lin, Xiaoyu Liu, and Suchuan Dong. A gPAV-based unconditionally energy-stable scheme for incompressible flows with outflow/open boundaries. *Comput. Methods Appl. Mech. Engrg.*, 365:112969, 38, 2020.
- [54] Yuan Liu, Wenbin Chen, Cheng Wang, and Steven M. Wise. Error analysis of a mixed finite element method for a Cahn-Hilliard-Hele-Shaw system. *Numer. Math.*, 135(3):679–709, 2017.
- [55] J. Lowengrub and L. Truskinovsky. Quasi-incompressible Cahn-Hilliard fluids and topological transitions. R. Soc. Lond. Proc. Ser. A Math. Phys. Eng. Sci., 454(1978):2617–2654, 1998.
- [56] Xiangjun Meng, Zhonghua Qiao, Cheng Wang, and Zhengru Zhang. Artificial regularization parameter analysis for the no-slope-selection epitaxial thin film model. CSIAM Transactions on Applied Mathematics, 1(3):441–462, 2020.
- [57] Giulio Schimperna and Sergey Zelik. Existence of solutions and separation from singularities for a class of fourth order degenerate parabolic equations. *Trans. Amer. Math. Soc.*, 365(7):3799–3829, 2013.
- [58] J. Schöberl. C++11 Implementation of Finite Elements in NGSolve, 2014. ASC Report 30/2014, Institute for Analysis and Scientific Computing, Vienna University of Technology.
- [59] Jie Shen, Cheng Wang, Xiaoming Wang, and Steven M. Wise. Second-order convex splitting schemes for gradient flows with Ehrlich-Schwoebel type energy: application to thin film epitaxy. SIAM J. Numer. Anal., 50(1):105–125, 2012.
- [60] Jie Shen, Jie Xu, and Jiang Yang. The scalar auxiliary variable (SAV) approach for gradient flows. *J. Comput. Phys.*, 353:407–416, 2018.

- [61] Jie Shen, Jie Xu, and Jiang Yang. A new class of efficient and robust energy stable schemes for gradient flows. SIAM Rev., 61(3):474–506, 2019.
- [62] Jie Shen and Xiaofeng Yang. Numerical approximations of Allen-Cahn and Cahn-Hilliard equations. *Discrete Contin. Dyn. Syst.*, 28(4):1669–1691, 2010.
- [63] Jie Shen and Xiaofeng Yang. Decoupled, energy stable schemes for phase-field models of two-phase incompressible flows. SIAM J. Numer. Anal., 53(1):279–296, 2015.
- [64] C. Taylor and P. Hood. A numerical solution of the Navier-Stokes equations using the finite element technique. *Internat. J. Comput. & Fluids*, 1(1):73–100, 1973.
- [65] Yue Yan, Wenbin Chen, Cheng Wang, and Steven M. Wise. A second-order energy stable BDF numerical scheme for the Cahn-Hilliard equation. *Commun. Comput. Phys.*, 23(2):572–602, 2018.
- [66] Xiaofeng Yang. A novel fully-decoupled, second-order and energy stable numerical scheme of the conserved Allen-Cahn type flow-coupled binary surfactant model. Comput. Methods Appl. Mech. Engrg., 373:113502, 2021.
- [67] Xiaofeng Yang and Lili Ju. Linear and unconditionally energy stable schemes for the binary fluid-surfactant phase field model. Comput. Methods Appl. Mech. Engrg., 318:1005–1029, 2017.
- [68] Xiaofeng Yang, Jia Zhao, and Qi Wang. Numerical approximations for the molecular beam epitaxial growth model based on the invariant energy quadratization method. J. Comput. Phys., 333:104–127, 2017.
- [69] Zhiguo Yang and Suchuan Dong. An unconditionally energy-stable scheme based on an implicit auxiliary energy variable for incompressible two-phase flows with different densities involving only precomputable coefficient matrices. J. Comput. Phys., 393:229-257, 2019.
- [70] Zhiguo Yang and Suchuan Dong. A roadmap for discretely energy-stable schemes for dissipative systems based on a generalized auxiliary variable with guaranteed positivity. *J. Comput. Phys.*, 404:109121, 46, 2020.
- [71] Zhengru Zhang and Zhonghua Qiao. An adaptive time-stepping strategy for the Cahn-Hilliard equation. *Commun. Comput. Phys.*, 11(4):1261–1278, 2012.
- [72] Jia Zhao, Xiaofeng Yang, Yuezheng Gong, and Qi Wang. A novel linear second order unconditionally energy stable scheme for a hydrodynamic Q-tensor model of liquid crystals. Comput. Methods Appl. Mech. Engrg., 318:803–825, 2017.